buildings

MDPI

Article

CFD-Based Evaluation of Wind Comfort in High-Density Primary Schools: A Case Study of Planning Layouts in Shenzhen

Zehua Ji [1], Hongbo Zhang [1], Liying Shen [2], Jiantao Weng [3,*], Qing Chun [4], Jindong Wu [2] and Xiaoyu Ying [3,*]

[1] China Construction Science and Industry Corporation Ltd., Shenzhen 518067, China; jzhzjkg2020@163.com (Z.J.); 15615269082@163.com (H.Z.)
[2] College of Civil Engineering and Architecture, Zhejiang University, Hangzhou 310058, China; 22012125@zju.edu.cn (L.S.); jindongwu@zju.edu.cn (J.W.)
[3] School of Spatial Planning and Design, Hangzhou City University, Hangzhou 310015, China
[4] School of Architecture, Southeast University, Nanjing 210096, China; cqnj1979@163.com
* Correspondence: wengjt@hzcu.edu.cn (J.W.); yingxiaoyu@hzcu.edu.cn (X.Y.)

Abstract

In Shenzhen, a high-density city facing severe land scarcity, the proliferation of compact primary school campuses poses significant challenges to the outdoor wind environment, which is crucial for outdoor thermal comfort in a hot–humid climate. This study employs Computational Fluid Dynamics (CFD) to systematically evaluate wind comfort across a range of high-density primary school layouts. Typical design proposals are classified and analyzed based on three key planning aspects: education building forms, courtyard openness, and sports field configuration. Wind comfort area ratio and static wind zone area ratio are adopted as key performance indicators to evaluate outdoor wind performance. The findings demonstrate that decentralized teaching building forms, multi-courtyard layouts with openings oriented towards the prevailing summer wind, and juxtaposed sports field placement significantly enhance outdoor ventilation and comfort. Additionally, positioning the main entrance on the windward side and incorporating elevated voids or terraces to form coherent ventilation corridors are effective design strategies. This research provides theoretical guidance for designing high-density school campuses in hot–humid southern China.

Keywords: high-density campus; wind environment; hot–humid climate; site planning; Computational Fluid Dynamics (CFD)

1. Introduction

In recent years, rapid urbanization in China has spurred substantial expansion in first-tier cities such as Beijing, Shanghai, Guangzhou, and Shenzhen. According to the Shenzhen Bureau of Statistics, the city's resident population reached 17.98 million in 2024, representing an increase of 4.81 million compared to 2014 (13.17 million). This reflects a total growth of 36.52% over the decade, with an average annual growth rate of 3.16% [1]. This population surge has intensified pressures on urban spatial layout, particularly in Shenzhen, which possesses the smallest total land area and the lowest per capita land availability among China's first-tier cities (as shown in Table 1). In response, the city has been actively pursuing strategies for intensive and refined urban development under high-density constraints. These demographic shifts have severely strained the development of school in downtown. In 2022, Shenzhen identified "increasing the development of quality school places" as one of its top ten key livelihood initiatives, with plans to provide

Academic Editor: Rafik Belarbi

Received: 8 December 2025
Revised: 24 January 2026
Accepted: 6 February 2026
Published: 10 February 2026

200,000 new basic education spaces and renovate or expand 178 educational institutions including nested, primary and secondary schools. Building upon the strategic needs outlined in previous urban studies [2], this research addresses the emerging paradox of school expansion under land scarcity. Specifically, it seeks to determine how primary school campuses can be designed to accommodate more classes and high floor area ratios without compromising the environmental and spatial quality essential for education.

Table 1. Land resources and population data of first-tier cities in China.

Name of City	Urban Area (km^2)	Number of Resident Population (10,000)	Land Area per Capita (m^2/Person)
Beijing	16,410.50	2189.30	749.55
Shanghai	6340.50	2487.10	254.91
Guangzhou	7434.00	1867.66	398.04
Shenzhen	1997.50	1343.88	148.64

To alleviate the contradiction between scarce per capita land resources and the growing demand for high-density school construction, architects have begun exploring new spatial paradigms for campus design. Among these efforts, the "Shenzhen's New School Initiative"—a design competition seeking proposals for multi-layered, high-density, composite urban campuses within the existing planning framework [3]—has been held consecutively from 2018 to 2022. The initiative has yielded a number of exemplary design proposals, some of which achieve floor area ratios exceeding 3.5, attracting significant attention from various sectors of society.

Shenzhen experiences a southern subtropical monsoon climate characterized by long summers, short winters, and abundant rainfall, with hot and humid conditions prevailing throughout most of the year. The high frequency of static wind exacerbates the stifling heat, underscoring the importance of adequate natural ventilation to improve outdoor thermal comfort [4]. In high-density urban areas of Shenzhen, wind speeds are generally low at the macro scale, limiting overall ventilation and heat dissipation capacity [4]. This often leads to the formation of eddies and wind shadows around buildings, impairing pedestrian comfort and hindering pollutant dispersion. At the micro scale, localized wind acceleration can cause discomfort and even hazardous conditions [5]. Furthermore, intensive land use and irregular site boundaries constrain campus layout, causing significant impacts on wind speed and direction at the pedestrian level. These factors contribute to drastic fluctuations in the outdoor wind environment, adversely affecting both wind comfort and air quality [6].

In this case, achieving a balance between spatial quality and wind comfort has become an urgent issue in the planning of high-density school campuses in Shenzhen. Flexible and varied site planning not only enriches students' spatial experience and encourages diverse activities but also enhances their perception of dynamic spatial aesthetics. Moreover, a comfortable outdoor wind environment in hot–humid climates can promote the physical and mental well-being of students and teachers. Passive design strategies aimed at enhancing natural ventilation can also reduce reliance on air-conditioning systems [7] and lower urban energy consumption [8,9]. Therefore, this study seeks to identify design strategies and methodologies for high-density campuses that achieve spatial quality with wind comfort, guided by these dual objectives.

This study makes the following technical contributions:

First, it focuses specifically on high-density primary school campuses, selecting representative cases from the "Shenzhen's New School Initiative" to form a substantial sam-

ple set. This approach allows the derivation of broadly applicable insights from case study analysis.

Second, it conducts a comparative study of campus building layout typologies and morphological scales, summarizing characteristic elements of school building clusters in high-density environments. By integrating multiple real cases through vertical and horizontal analysis, this study proposes comprehensive strategies for improving the wind environment.

Third, it investigates the relationship between campus building layout patterns and physical environmental performance, proposing layout configurations that enhance wind comfort and climate adaptability. These findings offer design strategies and references for architects at the preliminary design stage, enabling a greater focus on spatial quality and human comfort.

The remainder of this paper is structured as follows: Section 2 reviews the relevant literature and states research objectives; Section 3 outlines the research approach and methodology; Section 4 presents the numerical simulation process and analyzes the results; Section 5 discusses the findings; and Section 6 concludes this study and notes its limitations.

2. Literature Review

Faced with the severe scarcity of land in Shenzhen's urban centers, along with the growing demand for compulsory education facilities and high-density school construction, many schools have turned to significant upgrades and renovations on limited campus sites. Common intensification strategies include increasing density through urban renewal and demolition, adopting perimeter block configurations to maximize site utilization, and enhancing spatial efficiency by reconfiguring teaching building morphologies. Additionally, strategies such as creating multi-level courtyards and repositioning sports fields—whether through sinking, elevating, or integrating them with teaching volumes—are employed. All these measures are implemented in strict compliance with current design codes and site constraints. Compared with conventional campuses, high-density campuses are typically organized around several activity hubs at different heights, with circulation spaces closely integrated with teaching and activity areas, forming a vertically layered campus environment. However, the resulting stacking of building volumes and compression of outdoor spaces often lead to inadequate overall ventilation and localized airflow obstruction in outdoor campus spaces at the pedestrian level. The impact of campus layout on the wind environment has been increasingly examined by scholars both in China and internationally [6,10].

2.1. Morphological Changes in Teaching Buildings and Their Impact on the Wind Environment

In conventional campuses, teaching buildings are typically arranged in north–south-oriented rows with dispersed functional modules connected by corridors, due to the relatively fixed shape, scale, and quantity of basic teaching units, as well as regulations on daylighting and noise control. In contrast, for high-density primary and secondary schools, scholars have categorized teaching building forms based on functional integration intensity into types such as continuous corridor, linear, split-level sandwich, and centralized integral layouts [10].

In high-density campuses, teaching buildings often integrate multiple functional modules and utilize vertical stacking to meet spatial demands. This configuration, however, can easily cause airflow to form vortices or generate excessively high outdoor local wind speeds. Issues such as wind tunnel effects in corridors also contribute to unstable wind conditions. Research on the wind environment around teaching buildings includes analyses of architectural functional design in specific cases to derive ventilation strategies

for campuses [11–13]; simulations of classroom wind environments to identify effective measures for improving indoor ventilation [14]; and investigations into the relationship between classroom plan layout, wind angle, and ventilation effectiveness [15]. Most of these studies, however, focus on individual cases, operate at the master plan scale, and concentrate primarily on the indoor wind environment of teaching buildings.

2.2. Changes in Courtyard Form and Their Impact on the Wind Environment

Primary school campuses require ample outdoor spaces to support students' physical and mental health. These include sports fields, courtyards, outdoor activity platforms, and corridors. Some scholars classify high-density campus building layouts by courtyard type into circular inner courtyard, large composite, and courtyard agglomeration forms [16]. The high enclosure and density of such layouts, along with complex inter-building obstruction and overlapping courtyards, tend to limit natural ventilation, resulting in large wind shadow and stagnant air zones within courtyards.

Research on campus courtyard wind environments has shown that increasing the height-to-width ratio of parallel courtyards within a range of 0.5–2.0 (dimensionless) can be beneficial to airflow conditions [17]. Other studies have examined the relationship between courtyard opening orientation, courtyard combination, size ratio, and wind performance, concluding that east-facing openings and east–west courtyard alignment tend to yield better wind environments, while the area ratio between courtyards has limited impact [18]. However, most existing studies focus on the scale, proportion, and layout of conventional low-density campus courtyards, with limited attention paid to the particularities of high-density courtyard configurations.

2.3. Changes in Sports Field Layout and Their Impact on the Wind Environment

As the largest outdoor activity space on primary and secondary school campuses, the size and orientation of sports fields are typically specified in design standards [19]. The design of shared activity spaces also affects the quality and type of children's recess activities, as cross-level movement can hinder timely return to classrooms [20]. The "New Campus Project" explores approaches such as raising, sinking, deforming, and decentralizing sports fields. Compared with traditional layouts, the relationship between sports fields and teaching buildings in high-density campuses involves both two-dimensional and three-dimensional representations. On plan, adjacency to or insertion into teaching buildings may lead to ventilation issues due to overshadowing by upper structures. In this section, vertical repositioning redefines the layering of outdoor activity spaces, and the creation of multiple surfaces [21] complicates the spatial organization. Most existing studies focus on architectural forms, with limited consideration of how sports field layout integrates into the overall campus plan.

2.4. Limitations of Existing Studies

In general, most current studies use individual design cases as starting points to derive climate-adaptive design strategies. However, due to significant differences in environmental conditions and design concepts across cases, the resulting strategies tend to be context-specific and lack generalizability. Moreover, existing research focuses largely on indoor classroom ventilation [22], with insufficient attention paid to the relationship between outdoor wind environments, site ventilation, and building layout design in high-density campuses. Furthermore, studies often focus excessively on the morphological characteristics of individual buildings, paying little attention to the distinctive courtyard layouts in high-density campuses. There is also a lack of systematic research into the correlation between the overall campus spatial layout—including the siting of sports

fields—and wind performance, along with a shortage of specific ventilation strategies tailored to high-density campus conditions.

This paper addresses these gaps by examining recent award-winning high-density campus proposals in Shenzhen. Through analysis and generalization of formal and scalar attributes, and by comparing multiple schemes and evaluating wind comfort performance case by case, it derives ventilation strategies for high-density primary school campuses across three aspects: the degree of intensification in teaching building form, the openness of courtyard layout, and the configuration of sports fields. The findings provide a guideline for the layout design of high-density primary school campuses in hot–humid southern China, with an emphasis on outdoor wind comfort.

3. Research Approach and Methodology

This study employs a case study approach to identify and quantify morphological factors related to building layouts from a series of high-density campuses. The most representative cases were selected for modeling and computational analysis. Computational Fluid Dynamics (CFD) simulations were used to assess the wind environment, and wind comfort indices were applied to evaluate the performance of each layout, leading to the derivation of corresponding environmental improvement strategies.

3.1. Case Selection

According to the Shenzhen Statistical Yearbook 2022 [23], among the three types of schools—general secondary schools, kindergartens, and primary schools—primary schools experienced the fastest growth in both student enrollment and average student capacity, accompanied by the most severe shortage of school placements. Therefore, primary school campuses were selected as the focus of this study.

The Shenzhen's New School Initiative design competition, which explores intensive campus layout models beyond the constraints of existing design codes, provides a representative sample for analysis. A total of 11 primary school design proposals were chosen based on their typical teaching building forms, courtyard types, and sports field layouts, while maintaining consistency in class size and sports field specifications. Case studies were conducted to summarize and compare their economic and technical indicators, site plan layouts, and scales, as detailed in Tables 2 and 3.

Table 2. High-density primary school economic and technical indicators.

No.	Name	Volume Ratio	Site Area (m^2)	Capacitated Floor Area (m^2)	Number of Floors
1	Jinglong Primary School	3.43	9173.91	31,508.35	6 floors above ground
2	Xinsha Primary School	3.39	11,327.71	38,450.00	6 floors above ground
3	Xinzhou Primary School	2.70	10,568.57	38,564.60	6 floors above ground
4	Renmin Primary School	2.15	9550.83	25,301.17	6 floors above ground
5	Pingshan Jinlong Primary School	3.37	16,172.00	54,465.00	6 floors above ground
6	Hongling Experimental Primary School	3.54	10,062.00	33,721.00	6 floors above ground
7	Shixia Primary School	3.75	9428.00	31,568.00	5 floors above ground, partially 6 floors
8	Liyuan Primary School Zhongfu Campus	1.89	15,110.00	28,587.00	6 floors above ground
9	Meihong Primary School	2.57	10,800.00	27,801.00	6 floors above ground
10	Wulian Shang Yi Primary School	2.55	10,115.00	25,836.00	6 floors above ground
11	Fuqiang Primary School	2.55	11,190.18	28,538.00	4 floors above ground, partially 6 floors

Table 3. Spatial and functional characteristics of high-density primary school cases (figure source: Google Maps).

No.	Name	Site Planning	The Schematic Layout
1	Jinglong Primary School		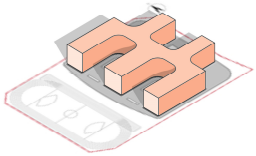
2	Xinsha Primary School		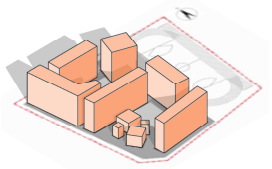
3	Xinzhou Primary School		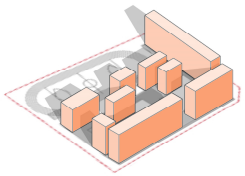
4	Renmin Primary School	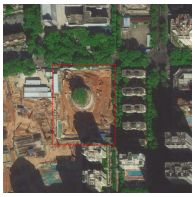	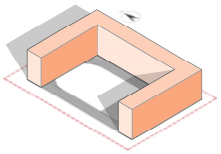
5	Pingshan Jinlong Primary School	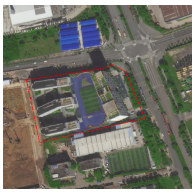	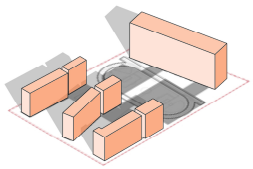
6	Hongling Experimental Primary School		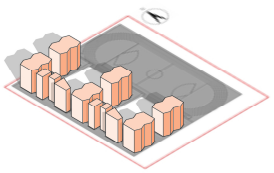
7	Shixia Primary School		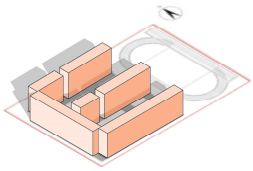

Table 3. *Cont.*

No.	Name	Site Planning	The Schematic Layout
8	Liyuan Primary School Zhongfu Campus		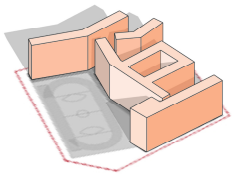
9	Meihong Primary School	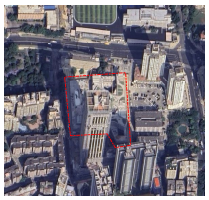	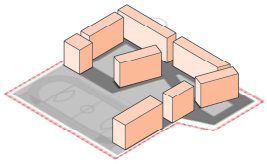
10	Wulian Shang Yi Primary School		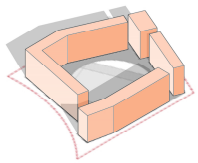
11	Fuqiang Primary School		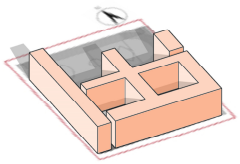

Observations indicate that sports fields are predominantly oriented north–south or at a slight offset, and most schemes feature a fully elevated second floor to accommodate the sports field overhead, thereby intensifying spatial organization. Key morphological elements influencing campus layout were categorized as follows:

- Teaching group layout (including building depth, building form, and corridor type of teaching units);
- Courtyard form (including number of courtyards and degree of enclosure);
- Sports field layout (including location, orientation, relationship to teaching groups, and relative orientation).

These elements collectively characterize the intensification of teaching group form, the openness of courtyard form, and the spatial relationship between sports fields and teaching groups, as summarized in Table 4.

Table 4. High-density primary school general plan layout form and scale.

No.	Name	Depth of the Building (m)	Teaching Building Morphology	Teaching Unit Corridor Form	Number of Courtyards	Courtyard Enclosure	Sports Field Location	Sports Field Orientation	Relationship with the Teaching Group	Relative Teaching Group Orientation
1	Jinglong	18.0	Staggered ranks	Double-side outer corridor	3	Three-sided	On the ground	N-S	Placed side by side	On the west side
2	Xinsha	15.0	Linear surround	Double-side outer corridor	2	Full	On the second floor	N-S	Placed side by side	On the east side
3	Xinzhou	13.5	Enclosed inner courtyard	Single-side outer corridor	2	Full	On the second floor	W-E	Placed side by side	On the north side
4	Renmin	12.0	Enclosed inner courtyard	Single-side outer corridor	1	Three-sided	On the third floor	N-S	Insertion	In Central
5	Pingshan Jinlong	12.6	Parallel ranks	Single-side outer corridor	0	openness	On the third floor	N-S	Placed side by side	On the east side
6	Hongling	15.0	Parallel ranks	Double-side outer corridor	2	Three-sided	On the third floor	N-S	Placed side by side	On the east side
7	Shixia	12.0	Staggered ranks	Single-side outer corridor	2	Three-sided, full	On the ground	N-S	Placed side by side	On the east side
8	Li yuan Zhongfu	12.0	Linear surround	Single-side outer corridor	3	Three-sided, full	On the second floor	NE-SW	Placed side by side	On the west side
9	Meihong	12.0	Enclosed inner courtyard	Single-side outer corridor	2	Three-sided, full	On the second floor	N-S	Placed side by side	On the west side
10	Wulian Shangyi	13.0	Enclosed inner courtyard	Single-side outer corridor	1	Full	On the second floor	NW-SE	Insertion	In Central
11	Fuqiang	12.0	Enclosed inner courtyard	Single-side outer corridor	2	Full	On the second floor	NW-SE	Placed side by side	On the northeast side

Among these, five high-density primary schools—Jinglong Primary School, Xinsha Primary School, Xinzhou Primary School, Renmin Primary School, and Pingshan Jinlong Primary School—were selected for detailed study. All five feature 36 classes and a standard 200 m sports field and represent typical variations in teaching building form, courtyard type, and sports field layout, as classified in Table 5.

Table 5. Classification of high-density primary school layout types and representative cases.

Classification			Representative Cases
Form of the teaching building	Lineage	Parallel determinant	Pingshan Jinlong
		Staggered ranks	Jinglong
	Continuous	Linear surround	Xinsha
		Composite enclosed	Xinzhou
	Centralized	Centralized Integral Type	Renmin
Courtyard form	Enclosed	Enclosed double courtyard	Xinzhou
	Three-sided enclosed	Single courtyard enclosed on three sides	Renmin
		Three sides enclosed double courtyard	Xinsha
		Three sides enclosed double courtyard	Pingshan Jinlong
	Semi-enclosed	Semi-enclosed multi-courtyard	Jinglong
Sports field layout	Stay on the ground	Co-location with teaching building	Jinglong
	Lifting to the second floor	Co-location with teaching building	Xinsha
			Xinzhou
	Lifting to the third floor	Co-location with teaching building	Pingshan Jinlong
		Insert into Teaching Building	Renmin

3.2. Simulation Condition Setting

The Computational Fluid Dynamics (CFD) software PHOENICS 2019 (CHAM Ltd., London, UK) has demonstrated reliable accuracy in reproducing overall wind environments [24,25]. Considering the characteristics of the research object and the requirements for both accuracy and computational efficiency, PHOENICS was selected for the numerical simulations in this study. Simulation conditions were configured in accordance with the *Testing and Assessment Standard for Building Wind Environment* [26] issued by the Guangdong Provincial Department of Housing and Urban-Rural Development in 2019, incorporating benchmark settings validated through prior simulations [27] and the latest technical guidelines for outdoor wind environment simulation [28,29].

3.2.1. Initial Wind Conditions

Shenzhen's natural wind environment is characterized by its coastal location, limited inland area, and high annual frequency of calm winds. Inflow wind conditions were determined based on multiple sources: the perennial wind frequency rose diagram for Shenzhen, the annual average wind speed records from the Shenzhen National Basic Meteorology Station (1990–2022) [4], and the *Shenzhen Climate Bulletin 2022* [4]. As the prevailing wind direction in summer differs from the annual dominant direction, and

buildings in hot–humid regions prioritize ventilation and cooling in summer, the summer dominant wind direction was selected as the primary orientation rather than the annual prevailing wind. The initial wind conditions were set as follows:

- Summer: dominant wind direction 135° (SE), with an average wind speed of 2.7 m/s at the 10 m reference height.
- Winter: dominant wind direction 22.5° (NNE), with an average wind speed of 3.0 m/s at the 10 m reference height.

3.2.2. Computational Domain

The blockage rate, defined as the ratio of the windward projected area of the model to the cross-sectional area of the computational domain, should remain below 3% according to wind tunnel experiment standards [30,31]. Following recommendations from existing studies [29,32,33], lateral and top boundaries were set at a distance of at least 5H from the building, and the outflow boundary at least 10H downstream, where H represents the height of the target building. Based on the volumetric scale of the studied objects, the computational domain dimensions were set to 500 m (x) × 500 m (y) × 150 m (z), consistent across all models.

3.2.3. Grid Settings

In accordance with Franke et al. [34], at least ten grid cells were applied along each building side, and a minimum of three cells were maintained at pedestrian-level heights (1.5–2 m above ground). A grid independence test was conducted (see Figure 1 and Table 6), confirming grid independence with a relative error of 0.3% within the grid count range of 2.3×10^5 to 7.3×10^5. The grid was locally refined with a transition ratio of 1.2. Dense grid sizes in the X–Y plane were set to 2 m, while the Z-direction used a gradually coarsening grid from bottom to top. The final grid configuration consisted of 102 × 90 × 32 cells, totaling 293,760 cells.

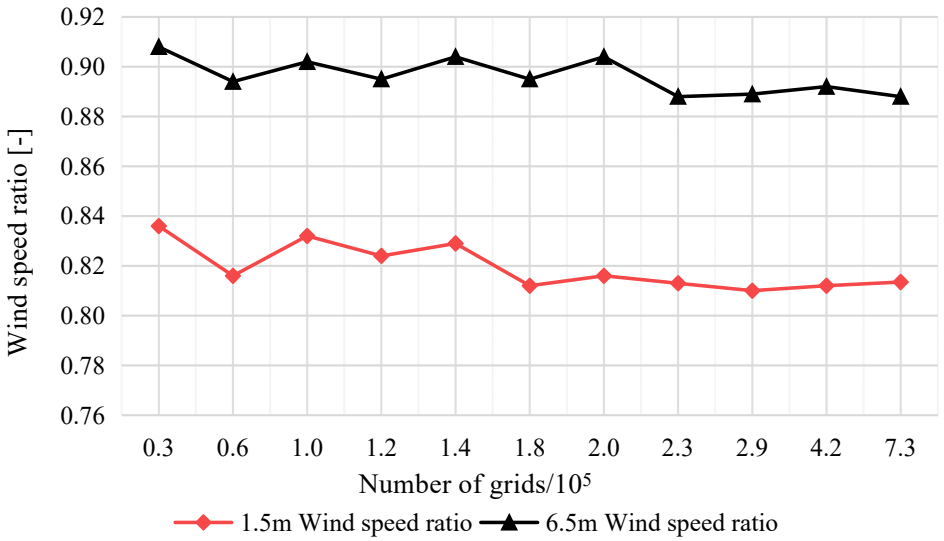

Figure 1. Grid independence verification.

Table 6. Comparison of grid sizes.

Grid Size (m)			Number of Girds
X	Y	Z	
10	10	0.5	0.3×10^5
8	8		0.6×10^5
6	6		1.0×10^5
5	5		1.2×10^5
4	4		1.4×10^5
3	3		1.8×10^5
3	2.5		2.0×10^5
2.5	2.5		2.3×10^5
2	2		2.9×10^5
1.5	1.5		4.2×10^5
1	1		7.3×10^5

3.2.4. Boundary Conditions

Based on the *Standard for Green Performance Calculation of Civil Buildings* [35] and the *Testing and Assessment Standard for Building Wind Environment* [26], terrain type and wind field parameters were defined as follows. The inlet boundary was set as a velocity inlet, the top and side boundaries as symmetry planes, and the ground and building surfaces as no-slip walls. Considering the high building density in Shenzhen's urban areas, the ground surface roughness was set to 0.30, corresponding to "dense mid- to high-rise building areas with undulating terrain."

3.2.5. Turbulence Model and Parameters

The standard k–ε model has been shown to provide accurate predictions of reattachment distances behind buildings near the ground [27] and requires less computational time. It is suitable for simulating wind fields at pedestrian level (1.5 m height) using a second-order upwind discretization scheme.

The standard k–ε model, originally proposed by Launder and Spalding [36,37], is governed by the following equations:

$$\frac{\partial U_i}{\partial x_i} = 0 \tag{1}$$

$$U_j \frac{\partial U_i}{\partial x_i} = -\frac{1}{\rho}\frac{\partial P}{\partial x_i} + \frac{\partial}{\partial x_j}\left(\mu \frac{\partial U_i}{\partial x_j}\right) + \frac{\partial}{\partial x_j}\left(-\overline{u_i u_j}\right) \tag{2}$$

where U represents the mean velocity component; x_i, x_j denote coordinate directions; and $\overline{u_i u_j}$ is the Reynolds stress term. The standard k–ε model relates the Reynolds stress to the mean velocity gradient as

$$-\overline{u_i u_j} = 2C_\mu k s_{ij} - \frac{2}{3} k \delta_{ij} \tag{3}$$

Here, C_μ is an empirical constant, and δ_{ij} is the Kronecker delta. The transport equations for turbulent kinetic energy k and dissipation rate ε are

$$U_j \frac{\partial k}{\partial x_j} = U_j \frac{\partial}{\partial x_i}\left[\left(\mu + C_k \frac{k^2}{\varepsilon}\right)\frac{\partial k}{\partial x_j}\right] - \overline{u_i u_j}\frac{\partial U_i}{\partial x_j} - \varepsilon \tag{4}$$

$$U_j \frac{\partial \varepsilon}{\partial x_j} = \frac{\partial}{\partial x_j}\left[\left(\mu + C_\varepsilon \frac{k^2}{\varepsilon}\right)\frac{\partial \varepsilon}{\partial x_j}\right] - C_{\varepsilon 1}\frac{\varepsilon}{k}\overline{u_i u_j}\frac{\partial U_i}{\partial x_i} - C_{\varepsilon 2}\frac{\varepsilon^2}{k} \tag{5}$$

where μ is the fluid kinematic viscosity. The model constants C_μ, C_k, C_ε, $C_{\varepsilon 1}$, and $C_{\varepsilon 2}$ are set to 0.09, 0.09, 0.07, 1.44, and 1.92, respectively [36].

The standard k–ε model assumes isotropic turbulent viscosity (i.e., C_μ is a constant). In contrast, the Realizable k–ε model, developed by Shih et al. [38], offers improved performance for simulating boundary layers, flows around blunt bodies, secondary flows, and curved wall boundaries [36]. The term "Realizable" implies that the model satisfies certain mathematical constraints on the Reynolds stresses, consistent with the physics of turbulent flows, which enhances its accuracy for complex flow patterns commonly found in the built environment, such as flow separation and recirculation around building clusters.

For the specific application of pedestrian-level wind environment simulation around buildings, the Realizable k–ε model has been extensively validated and is widely regarded as a robust and reliable choice. It demonstrates a favorable balance between computational efficiency and simulation accuracy for architectural and urban-scale studies [39–41]. Therefore, the Realizable k–ε model was adopted in this study.

3.2.6. Convergence Criteria

The convergence criteria were defined as follows: a minimum of 5000 iterations, residuals below 1×10^{-4}, and an equation imbalance rate within 1% [42]. Simulations were considered converged when values at representative monitoring points stabilized or fluctuated around a constant value. The baseline simulation settings are summarized in Table 7.

Table 7. Baseline simulation condition settings.

	Working Condition	Parameters
Computational Domain		500 m (x) × 500 m (y) × 150 m (z)
Grid division		102 (x) × 90 (y) × 32 (z) = 293,760
Initial wind conditions	Summer	Southeast 135° (SE), V0 = 2.7 m/s
	Winter	Winter 22.5° north-northeast (NNE). V0 = 3.0 m/s
Boundary Conditions	Inflow boundary	Velocity inlet
	Outflow boundary	Free outflow
	Top and side boundaries	Symmetry
	Building surfaces	No-slip wall
	Ground surface	No-slip wall
Turbulence model		Realizable k-ε model
Number of iterations		>5000, or until convergence
Convergence criteria		Residuals < 1×10^{-4}

3.3. Distribution of Measurement Points

Measurement points were located in outdoor activity spaces characterized by relatively high pedestrian flow, frequent use, and longer dwell times. Given that the elevation of the sports field impacts the distribution of outdoor activity areas, two categories of points were defined: Type I points at a pedestrian height of 1.5 m above ground level, and Type II points at the elevated level of the sports field. Additionally, a designated measurement point (denoted as E) was placed at the campus entrance, where pedestrian concentration is highest (see Table 8).

Table 8. Distribution of measurement points across five schools.

Figure Legend	Jinglong Primary School	Xinsha Primary School
Measurement points Red line Building volume Corridor/Platform Athletic Field Location North arrow Dominant wind conditions	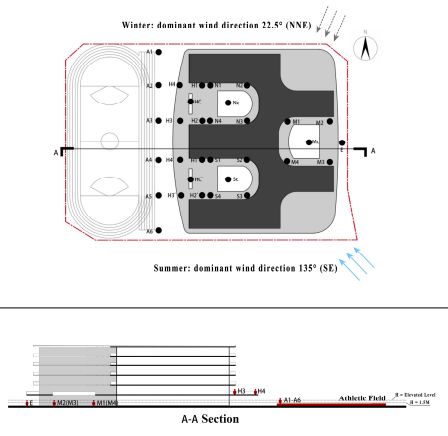	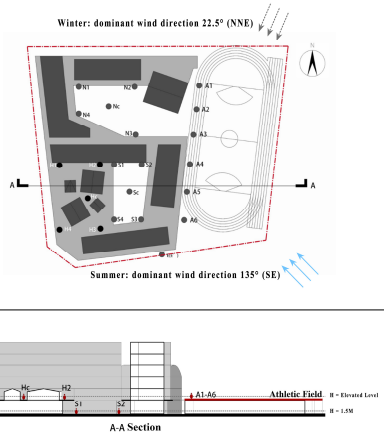
Xinzhou Primary School	**Renmin Primary School**	**Pingshan Jinlong Primary School**
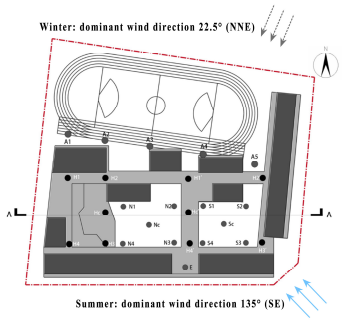	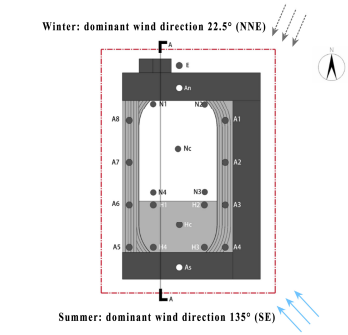	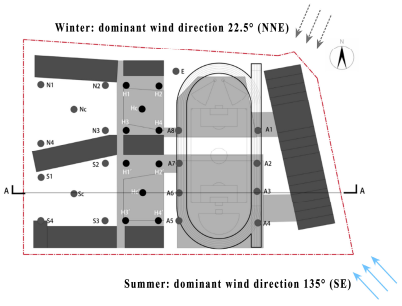

3.4. Wind Environment Evaluation Criteria

Within a certain wind speed threshold, the wind speed ratio around buildings tends to stabilize despite variations in the initial wind speed. Following urban wind environment evaluation guidelines for pedestrian-level conditions [43], four indices were adopted to assess the relative impact of different building layouts on the wind environment: wind speed ratio, standard deviation of wind speed ratio, wind comfort area ratio, and static wind zone area ratio.

3.4.1. Wind Speed Ratio

Wind speed ratio is defined as the ratio of the wind speed V_i at a pedestrian-level measurement point to the undisturbed incoming wind speed V_0. This ratio reflects the impact of buildings on the local wind field. Unlike absolute wind speed, the wind speed ratio is independent of variations in the incoming wind speed, allowing for a more objective comparison of ventilation conditions across measurement points. It is calculated as

$$R_i = \frac{V_i}{V_0} \tag{6}$$

where R_i is the wind speed ratio, V_i is the wind speed at the measurement point (m/s), and V_0 is the initial incoming wind speed (m/s).

3.4.2. Wind Speed Ratio Dispersion

The standard deviation of the wind speed ratio is used to characterize the variability in wind speed distribution among measurement points within a layout. It is calculated as

$$\sigma = \sqrt{\frac{1}{n}\sum_{i=1}^{n}(V_i - \mu)^2} \quad (7)$$

where V_i is the wind speed ratio at each measurement point, and μ is the mean wind speed ratio of all points. A smaller standard deviation indicates a more uniform wind speed distribution and a more stable wind environment.

3.4.3. Wind Comfort Area Ratio

The wind comfort area ratio is the proportion of the site area (within the red line) where the wind speed ratio falls within a comfortable range. It is expressed as

$$S = \frac{S_C}{S_F} \times 100\% \quad (8)$$

where S is the wind comfort area ratio, S_C is the area satisfying comfort wind speed criteria (m^2), and S_F is the total site area (m^2). A higher ratio indicates better overall wind comfort across the site.

3.4.4. Static Wind Zone Area Ratio

The static wind zone area ratio represents the proportion of the site where wind speeds fall below a specified threshold, indicating stagnant air conditions. It is calculated as

$$C = \frac{S_{sw}}{S_F} \times 100\% \quad (9)$$

where C is the static wind area ratio, S_{sw} is the static wind area (m^2), and S_F is the total site area (m^2).

3.4.5. Selected Wind Environment Evaluation Criteria

Based on pedestrian-level urban wind environment evaluation guidelines and adapted to the context of this study, the four indices described above are used to evaluate site ventilation, wind speed stability, and wind comfort, respectively. These criteria allow for a comprehensive assessment of how different building layouts impact various aspects of the wind environment, as summarized in Table 9.

Table 9. Wind environment evaluation indicators.

Evaluation Indicators	Wind Environment Characteristics	Range of Comfort Indicators
Average wind speed ratio	Site ventilation	0.5–1.67 in winter; 0.5–1.85 in summer
Wind speed ratio dispersion	Wind speed stability	Smaller values indicate greater stability
Wind comfort area ratio	Field wind comfort level	Wind speed 1.35–5.0 m/s (summer), 1.5–5.0 m/s (winter)
Static wind zone area ratio	Site static wind conditions	Wind speed < 0.3 m/s

Consistent with the findings of Janssen et al. [44] and related empirical studies in China [43], a wind speed ratio within the range of 0.5 to 1.5 is typically identified as the comfort threshold. However, in Shenzhen's hot–humid climate, enhanced natural ventilation is essential to mitigate summer heat stress, necessitating a contextual re-evaluation of

the upper limit. Cheng and Ng [45] also noted that wind speeds exceeding 5 m/s begin to cause pedestrian discomfort. Accordingly, the comfortable wind speed ratio ranges were defined as

- Winter: 0.5–1.67 (equivalent to 1.5–5.0 m/s);
- Summer: 0.5–1.85 (equivalent to 1.35–5.0 m/s).

While some engineering simulation software classifies wind speeds below 0.2 m/s as static wind zones—referencing the *Grage of Tropical Cyclones* (GB/T 19201-2006) [46]—this threshold is considered too low for assessing human comfort in building environments. Based on the Beaufort wind scale and thermal comfort considerations at pedestrian height, a wind speed <0.3 m/s is adopted here to define static wind zones [47]. The smaller the area ratio of the static wind zone, the better the overall ventilation of the scheme.

Regarding the impact of transient wind speed variations, it is acknowledged that natural wind is inherently unsteady. However, for a comparative evaluation of building layout patterns—which is the primary objective of this study—a steady-state simulation approach based on the representative average wind speed is a well-established and effective methodology [48,49]. This approach allows for a clear and controlled comparison of the relative performance of different architectural forms under a dominant, representative condition. While transient analysis could capture peak wind events, the comfort criteria adopted in this study (which set an upper wind speed limit) are designed to assess the prevalent wind environment experienced during typical weather conditions. Furthermore, addressing occasional extreme wind speeds often requires site-specific mitigation measures beyond the scope of layout optimization alone. Therefore, the use of steady-state simulation with mean wind speed inputs is deemed appropriate for deriving generalizable design strategies aimed at enhancing wind comfort under the most common and thermally critical scenarios in Shenzhen.

4. Results and Data Analysis

Wind environment indices for each case were obtained through PHOENICS simulations [24,25], with numerical results summarized in Table 10 and spatial distributions of comfort and static wind zones illustrated in Figure 2 using seasonal wind speed ratio ranges of 0.5–1.67 (dimensionless) for winter and 0.5–1.85 (dimensionless) for summer, while areas with wind speeds below 0.3 m/s were classified as static zones.

Table 10. Quantitative comparison of outdoor wind environment performance across five representative cases.

Name	Average Wind Speed Ratio [-]	Wind Speed Ratio Dispersion	Static Wind Zone Area Ratio	Wind Comfort Area Ratio
Jinglong	0.63	0.71	6.6%	58.0%
Xinsha	0.62	0.48	6.6%	55.7%
Xinzhou	0.54	0.50	18.0%	42.5%
Renmin	0.42	0.53	44.7%	17.6%
Pingshan Jinlong	0.69	0.52	24.5%	29.9%

[-] indicates a dimensionless quantity.

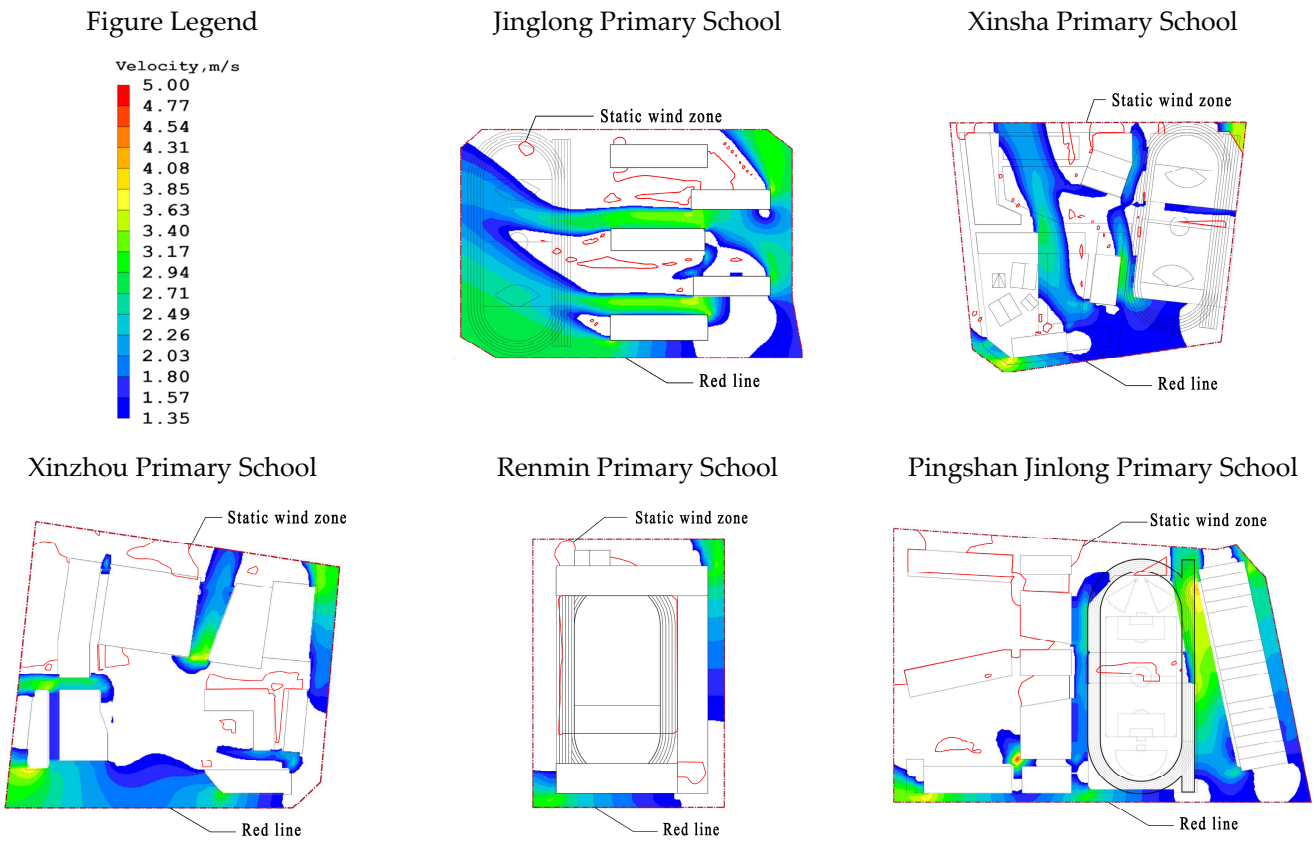

Note: The red dash line denotes the boundary of the school campus.

Figure 2. Distribution of wind comfort zones and static wind zone across five representative cases.

4.1. Overall Analysis

4.1.1. Site Ventilation

As shown in Table 10, the average summer wind speed ratios for Jinglong, Xinsha, Xinzhou, and Pingshan Jinlong Primary Schools all fall within the comfortable range (0.5–1.85), while Renmin Primary School's ratio of 0.42 falls slightly below the minimum threshold. Pingshan Jinlong Primary School demonstrates the highest ventilation efficiency, whereas Renmin Primary School shows the lowest.

Analysis of teaching building morphology intensification reveals that average wind speed ratios decrease in the order: parallel rows > continuous forms > centralized layouts, indicating that ventilation efficiency declines as building forms become more compact. Regarding courtyard openness, three-sided enclosed and semi-enclosed courtyards with openings facing incoming winds provide better ventilation, while reduced openness or misaligned openings impede airflow. Sports field configuration also significantly impacts ventilation; separated sports fields yield higher wind speed ratios than those nested into teaching buildings, and elevated fields generally exhibit poorer ventilation. Therefore, parallel teaching building placement, three-sided/semi-enclosed courtyards, and ground-level separated sports fields represent preferable configurations for ventilation.

4.1.2. Site Wind Comfort

Table 10 reveals an inverse relationship between wind comfort zone and static wind zone proportions across the five cases. Jinglong Primary School shows the highest wind comfort ratio, followed by Xinsha, Xinzhou, Pingshan Jinlong, and Renmin Primary Schools. Conversely, static wind zone percentages follow the opposite order: Renmin > Pingshan Jinlong > Xinzhou > Xinsha = Jinglong. Jinglong and Xinsha Primary Schools exhibit more

evenly distributed comfort zones forming consistent ventilation corridors, with minimal static zones located outside primary activity areas.

Teaching building intensification analysis indicates that as layouts transition from dispersed to compact, wind comfort areas decrease while static zones expand. Centralized layouts with nested sports fields show minimal comfort zones, as dense building placement create significant wind obstructions. Courtyard openness analysis demonstrates that as enclosure decreases, comfort zones expand while static zones contract. Multiple courtyards provide larger comfort areas and smaller static zones compared to single-courtyard configurations. Regarding sports field layout, separated configurations show decreasing comfort areas and increasing static zones as elevation increases, with ground-level locations providing optimal comfort conditions. Therefore, dispersed teaching building layouts, open multi-courtyards, and ground-level separated sports fields maximize wind comfort, while centralized layouts with nested sports fields should be avoided.

4.2. Wind Environment Improvement and Design Strategies

Based on comparative analysis of wind environment indices across morphological types, case-specific ventilation strategies were developed.

4.2.1. Main Entrance Placement Combined with Ground Floor Elevation

To shape the urban interface and meet the needs of sharing and evacuation, the main entrance plaza of the campus becomes a public space for cultural displays and crowds staying for a long time. The main entrance of Renmin Primary School is located on the north side of the building and has the lowest wind speed ratio of 0.17; the main entrance of Jinglong Primary School is located on the east side of the building and has a wind speed ratio of 0.81, which is relatively the highest among the five scenarios, as shown in Figure 3. Combined with the surrounding environment, functional layout, and other comprehensive factors, the main entrance is placed on the side of the dominant wind and combined with the ground floor elevation to obtain a more comfortable entrance wind environment.

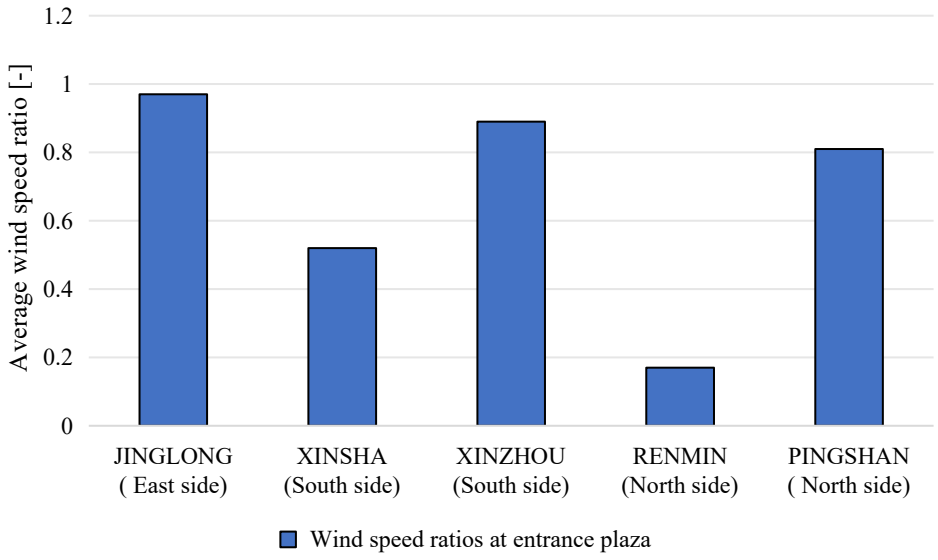

Figure 3. Comparison of wind speed ratios at main campus entrances across five schools.

4.2.2. East–West Volume Setbacks

Jinglong Primary School has the best ventilation and the best wind comfort on the site, but the lowest outdoor wind environment stability (Figures 4–6). As the sports field is located in the wind shadow area of the teaching building, the wind environment along the sports field is also more unstable, and the state of uneven regional distribution of the wind

environment still exists at the second-floor height. The wind speed ratios of the north side of the north courtyard and the north side of the south courtyard were the lowest among all measurement points, 0.07, 0.11, 0.12, and 0.27, respectively, all of which belonged to the static wind area, while the wind speeds of the measurement points on the south side of both courtyards were higher, which was caused by the misalignment of volume and mutual shading to form the narrow tube effect of wind. The wind environment on the north side of the courtyard is more uncomfortable than that on the south side of the courtyard. In the design, the wind shadow area between the wrongly moving volumes can be reduced by giving way in the east–west direction to avoid uneven distribution of wind speed in the courtyard due to the wind's narrow tube effect, while making the interconnected areas between volumes more permeable to meet the needs of landscape infiltration and students' outdoor activities on the same level.

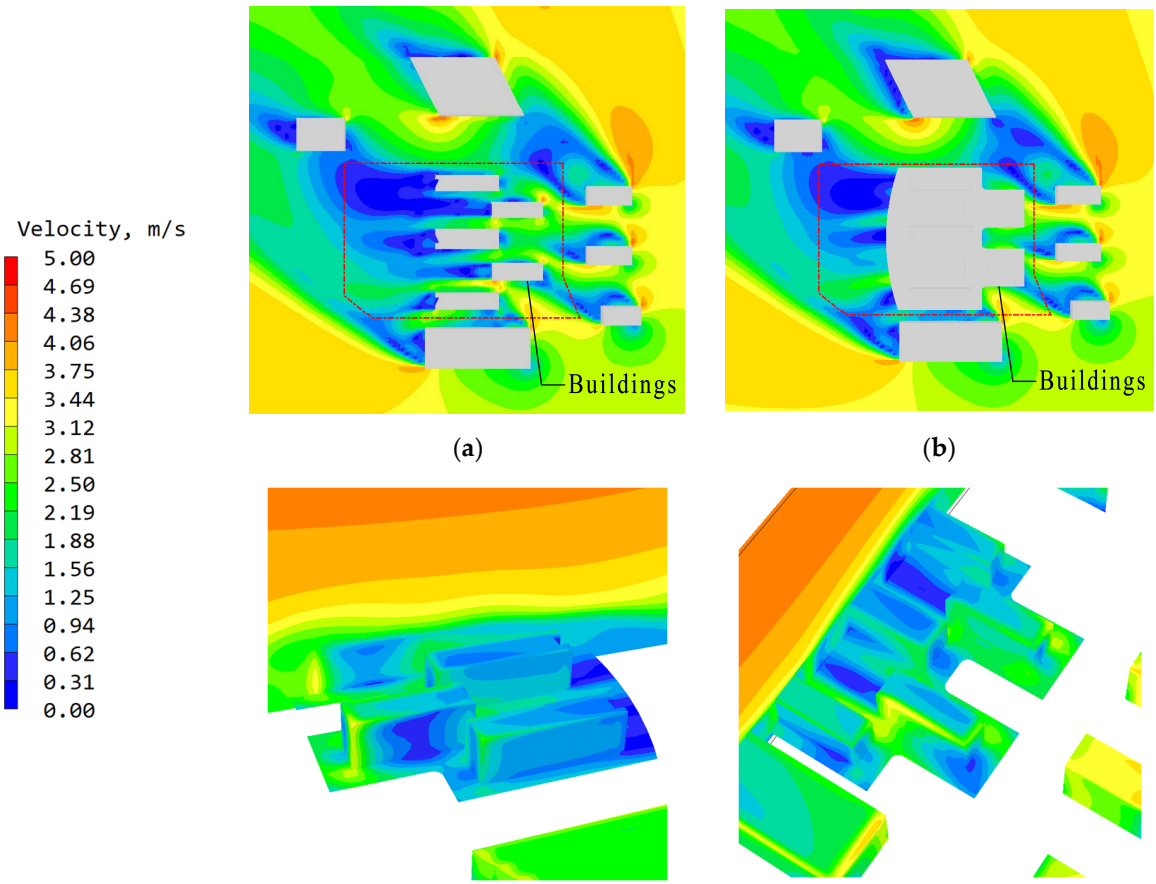

Note: The red dash line denotes the boundary of the school campus.

Figure 4. Multi-level and cross-sectional wind speed distributions of Jinglong Primary School. (**a**) Wind speed distribution at the ground pedestrian level; (**b**) wind speed distribution at the elevated activity platform level; (**c**) cross-sectional wind profile; (**d**) axonometric view with longitudinal section contours.

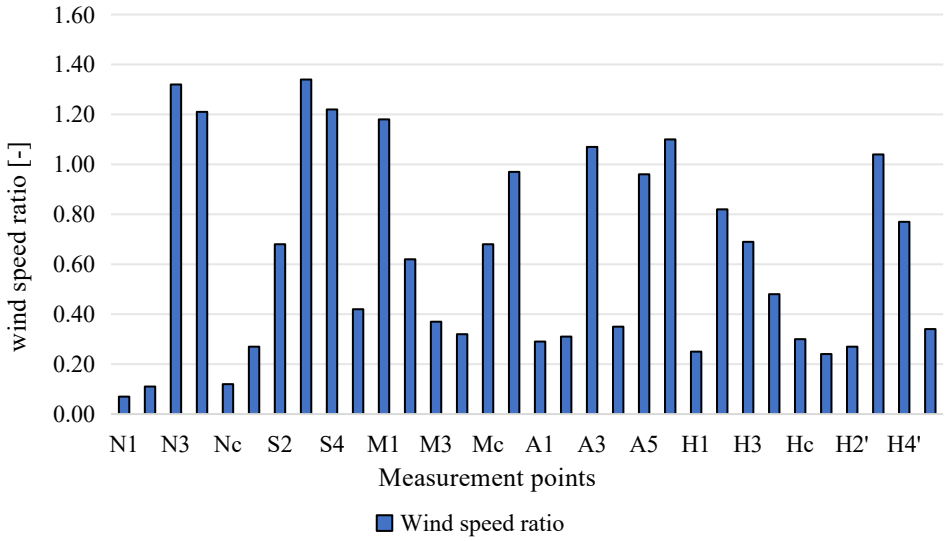

Figure 5. Comparison of wind speed ratios at different observation points of Jinglong Primary School in summer.

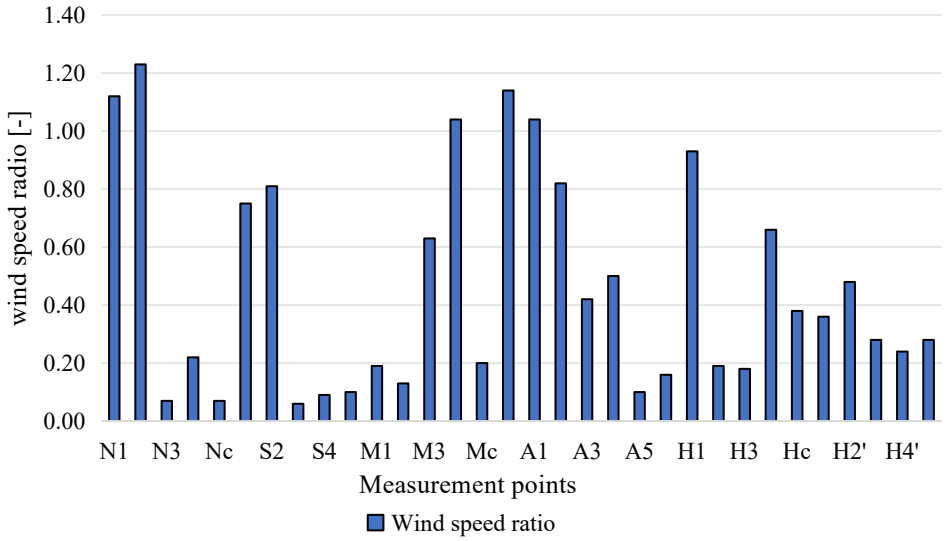

Figure 6. Comparison of wind speed ratios at different observation points of Jinglong Primary School in winter.

4.2.3. Enhanced Courtyard Openness to Prevailing Winds

The site ventilation, wind environment stability, and site wind comfort area ratio of Xinsha Primary School are better. The main volume of the building is "S-shaped", with linear surrounds enclosing two inner courtyards to the north and south, and the first-floor volume is partially elevated, with the main entrance located on the south side of the building. The sports field is elevated to the first-floor roof, located on the east side of the site. The outdoor activity platform is located on the west side of the second floor, which is open to the community and consists of four double-sloped volumes with different orientations, cutting the activity platform into irregular areas and significantly reducing the overall wind speed compared to the first-floor courtyard. The multi-directional courtyard is interesting, meets the activity psychology of primary school students, and also achieves better community openness, but the ventilation condition of the site is also more unstable than that of the regular-shaped courtyard.

From Figures 7–9, it can be seen that there is an obvious north–south through-wind corridor at the ground level, and the wind speed around the second-floor platform is

lower than that at its center. Additionally, due to the linear continuous enclosure of the teaching building, the north and south courtyards exhibit a wind speed decrease from the center to the periphery, accompanied by vortex phenomena. Increasing the openness of the courtyards on the east and south sides of the second floor and expanding the courtyard air intake area will result in a more stable and comfortable courtyard wind environment.

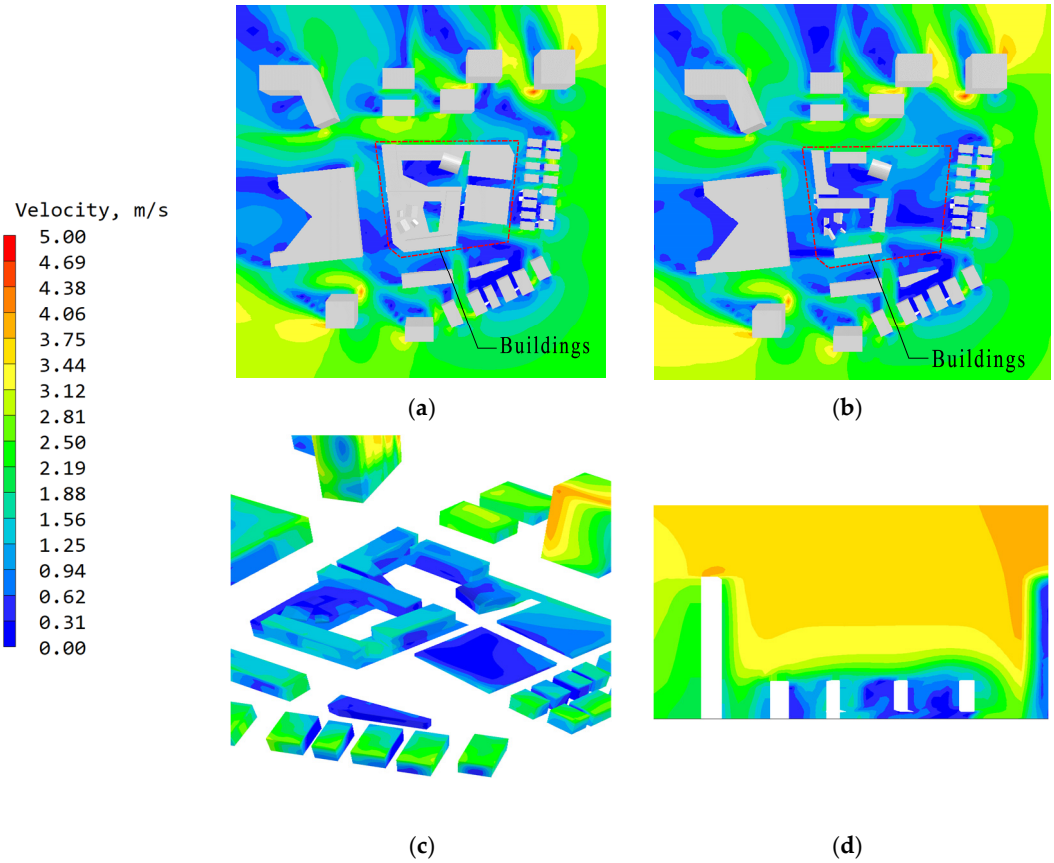

Note: The red dash line denotes the boundary of the school campus.

Figure 7. Multi-level and cross-sectional wind speed distributions of Xinsha Primary School. (**a**) Wind speed distribution at the ground pedestrian level; (**b**) wind speed distribution at the elevated activity platform level; (**c**) wind speed contours on building surfaces; (**d**) longitudinal wind profile.

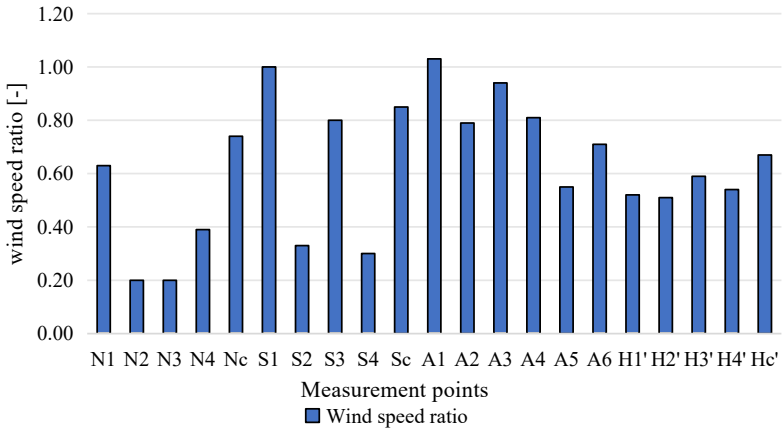

Figure 8. Comparison of wind speed ratios at different observation points of Xinsha Primary School in summer.

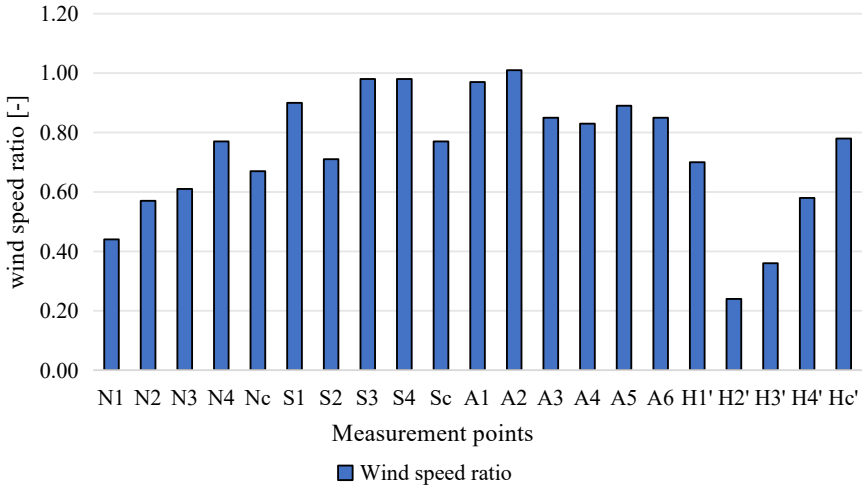

Figure 9. Comparison of wind speed ratios at different observation points of Xinsha Primary School in winter.

4.2.4. Windward Outdoor Activity Platforms

Xinzhou Primary School takes the consideration of physical properties such as lighting, noise reduction, and ventilation of campus buildings as the dominant factor in design decisions and the site ventilation efficiency, wind environment stability, and site wind comfort area ratio are used to follow the historical pattern of the original campus. The sports field is arranged east–west on the north side of the building volume and raised to the second floor. The main teaching units are enclosed in a figure-of-eight shape to form two inner courtyards in the west and east. The public activity space is cantilevered like a cascading box on the north side of the courtyard, and the main entrance to the campus is located on the south elevated level.

The wind environment in the west courtyard at ground level is generally better than that in the east courtyard, and the wind speed fluctuation in the west courtyard is smoother than that in the east courtyard (as shown in Figures 10–12). The wind environment of the corridor on the north side of the north and south main teaching unit volumes are at a more comfortable level. At the second-floor deck, the wind speed distribution is more uniform than at the first-floor courtyard. However, the wind speed ratio at measurement point H3' (shown in Figure 10) is particularly prominent, reaching 1.13, because this measurement point happens to be located at the opening where the dominant wind enters the courtyard in summer. If part of the outdoor activity platform can be left at the gap between the connected teaching units on the windward side to break the enclosure of the teaching building shape, it can help improve the situation of lower wind speed on the northeast side of the east courtyard (shown in Figure 11).

4.2.5. Ventilation Openings for Prevailing Winds

The site ventilation efficiency and site wind comfort area of Renmin Primary School is smaller compared to other programs, but the wind environment is more stable overall. Due to the red line requirement and the limitation of the original topography, to preserve the central woods, the sports field was decomposed and hollowed out in the middle, and the track was raised to the third floor and nested into the elevated floor of the centralized teaching building. The courtyard is enclosed on three sides in the shape of "C", forming a semi-open courtyard facing west on the first floor and a south activity platform on the third floor. The main entrance is located on the north side of the building.

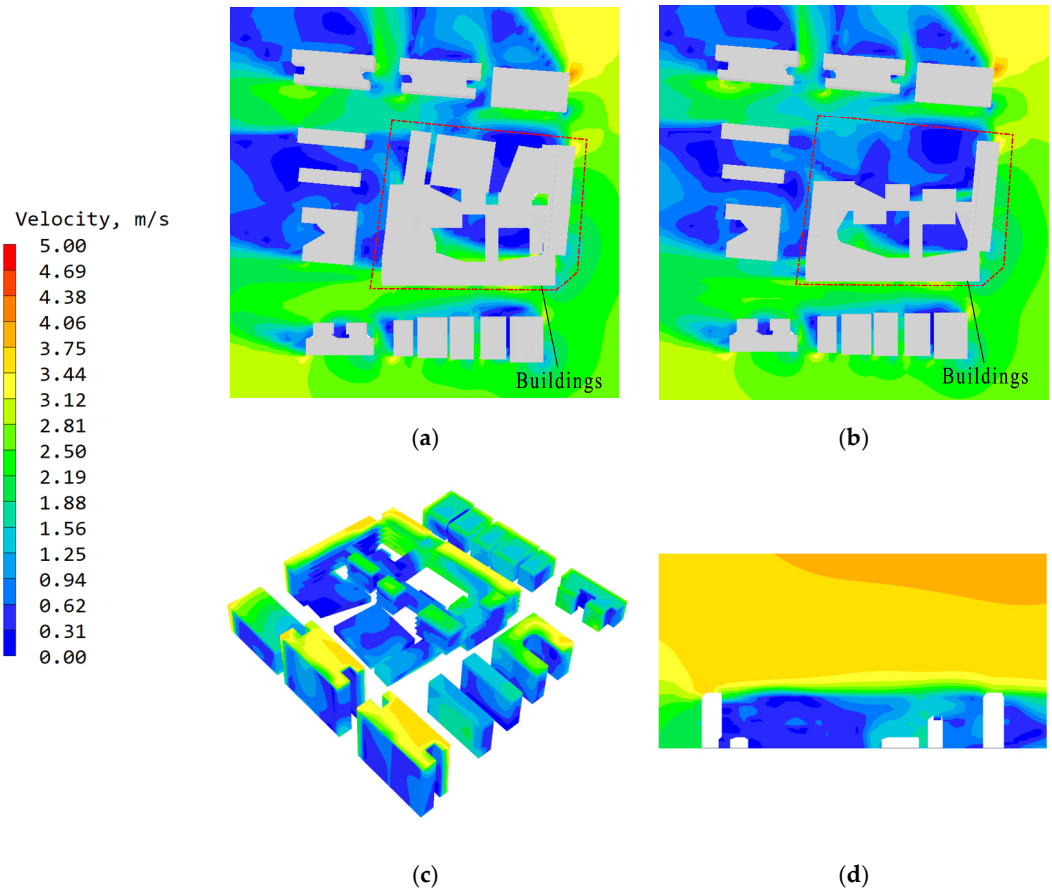

Note: The red dash line denotes the boundary of the school campus.

Figure 10. Multi-level and cross-sectional wind speed distributions of Xinzhou Primary School. (**a**) Wind speed distribution at the ground pedestrian level; (**b**) wind speed distribution at the elevated activity platform level; (**c**) wind speed contours on building surfaces; (**d**) longitudinal wind profile.

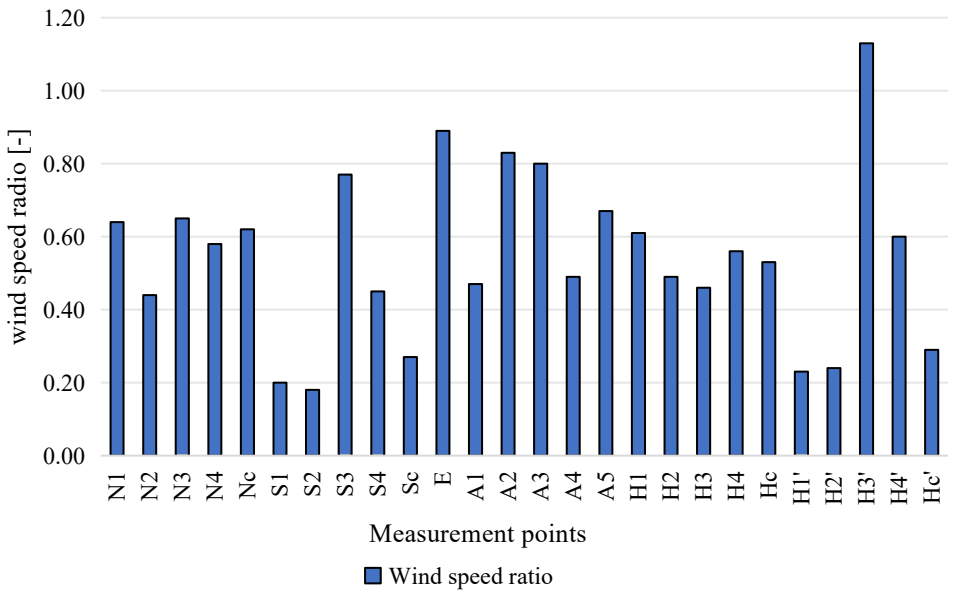

Figure 11. Comparison of wind speed ratios at different observation points of Xinzhou Primary School in summer.

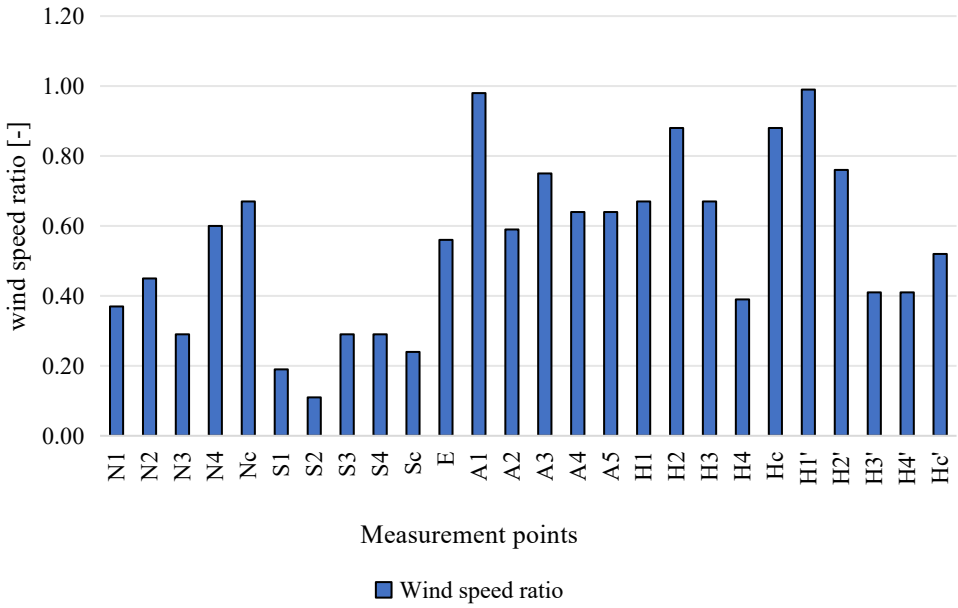

Figure 12. Comparison of wind speed ratios at different observation points of Xinzhou Primary School in winter.

Due to the more enclosed building form in the southeast corner, the trees are heavily shaded, and the sports field is covered above, the overall wind speed in the courtyard of the first floor of Renmin Primary School is stable at a low level, and all are in the static wind zone (as shown in Figures 13 and 14). Among the measurement points of the sports field, A3 and A4 are in the wind shadow area of the building on the southeast side, and the wind speed is 0.8 m/s and 0.28 m/s, respectively, while the ventilation improvement effect is especially obvious in the overhead corridor on the east side of the building against the north, as shown in Figures 13b and 15. If the overall orientation of the building is changed from the opening on the west side to the opening on the east side, overhead floors and outdoor platforms are set up on the east side of the first floor, and ventilation openings are set up in the dominant wind direction, The ventilation condition of the courtyard and the third-floor activity platform can be improved significantly.

4.2.6. North–South Ventilation Corridors in Teaching Groups

The site of Pingshan Jinlong Primary School has the best ventilation and better stability in an outdoor wind environment, but the wind comfort of the site is at a lower level in the layout where the teaching building and the sports field are separated. The row-like teaching building is located on the west side of the site, consisting of three rotated strips at a certain angle, connected by a connecting corridor on the east side, and enclosed by three sides into two courtyards on the north and south. The gymnasium, which has been raised to three levels, is located between the teaching and dormitory buildings and combined with the three-level activity platform to form a three-dimensional transportation hub.

From Figures 16–18, it can be seen that the north courtyard at the ground level is in the static wind area; the wind speed in the south courtyard increases significantly; the wind speed reaches the maximum at measurement point S3, which is located in the direction of the prevailing wind; and the ventilation opening narrows abruptly, resulting in a larger wind speed, but also makes the wind speed in the north courtyard lower overall. As shown in Figures 16b and 17, if the volume of the teaching building opens several north–south ventilation corridors, it will have an enhancing effect on the wind environment of the north courtyard at ground level. Since the sports field is located between the teaching building and the dormitory building, which makes the southeast side open, the wind environment

of the central activity platform is relatively good. The elevation of the sports field makes the ground level form clustering, if the large space is properly decomposed to form through multiple profile wind corridors, it will reduce the range of the ground-level static wind area and improve the wind comfort of the site.

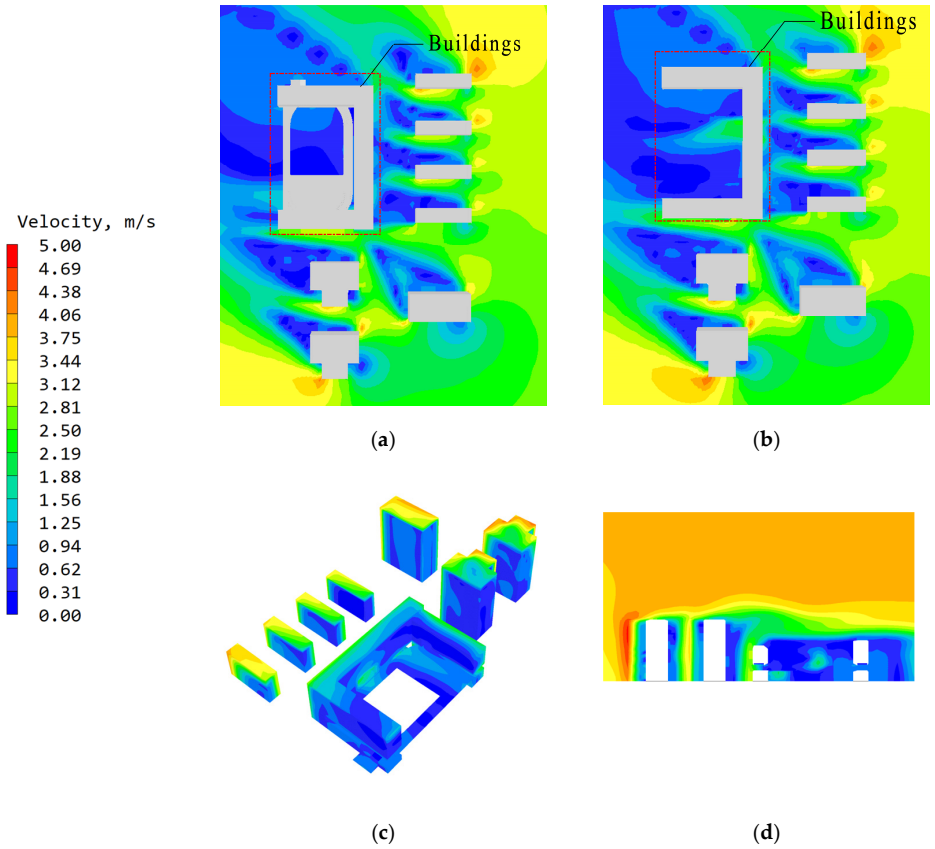

Note: The red dash line denotes the boundary of the school campus.

Figure 13. Multi-level and cross-sectional wind speed distributions of Renmin Primary School. (**a**) Wind speed distribution at the ground pedestrian level; (**b**) wind speed distribution at the elevated activity platform level; (**c**) wind speed contours on building surfaces; (**d**) longitudinal wind profile.

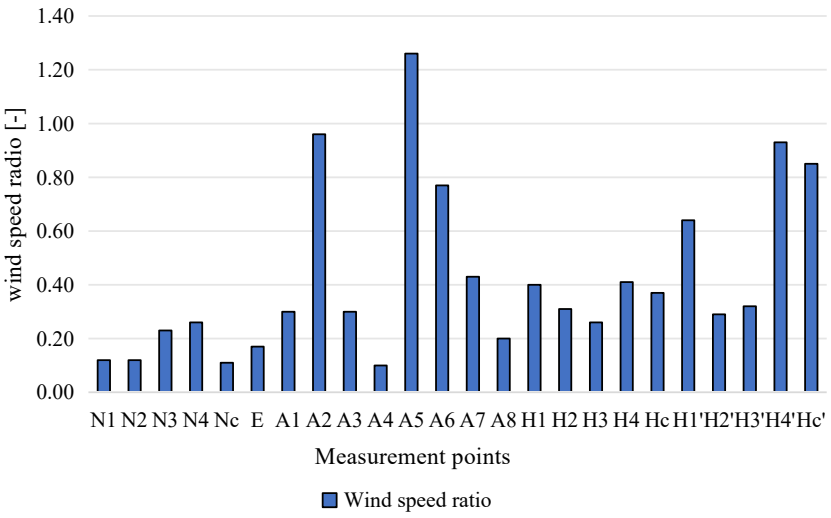

Figure 14. Comparison of wind speed ratios at different observation points of Renmin Primary School in summer.

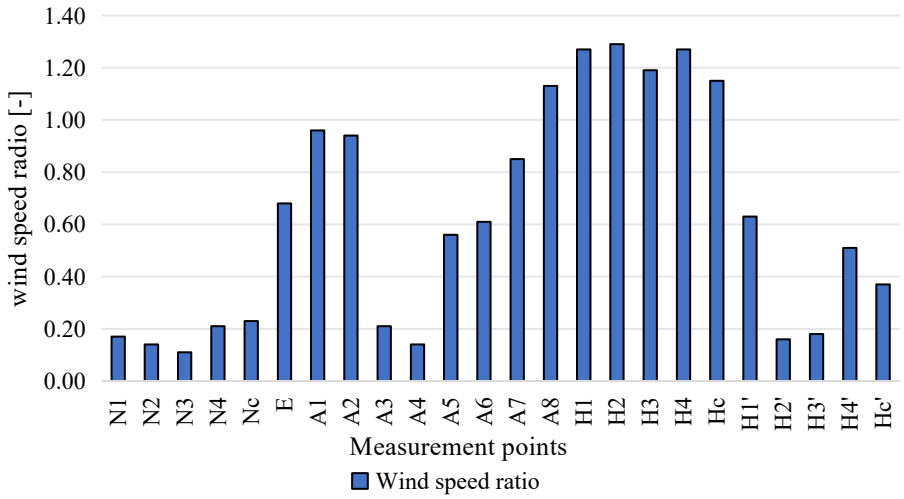

Figure 15. Comparison of wind speed ratios at different observation points of Renmin Primary School in winter.

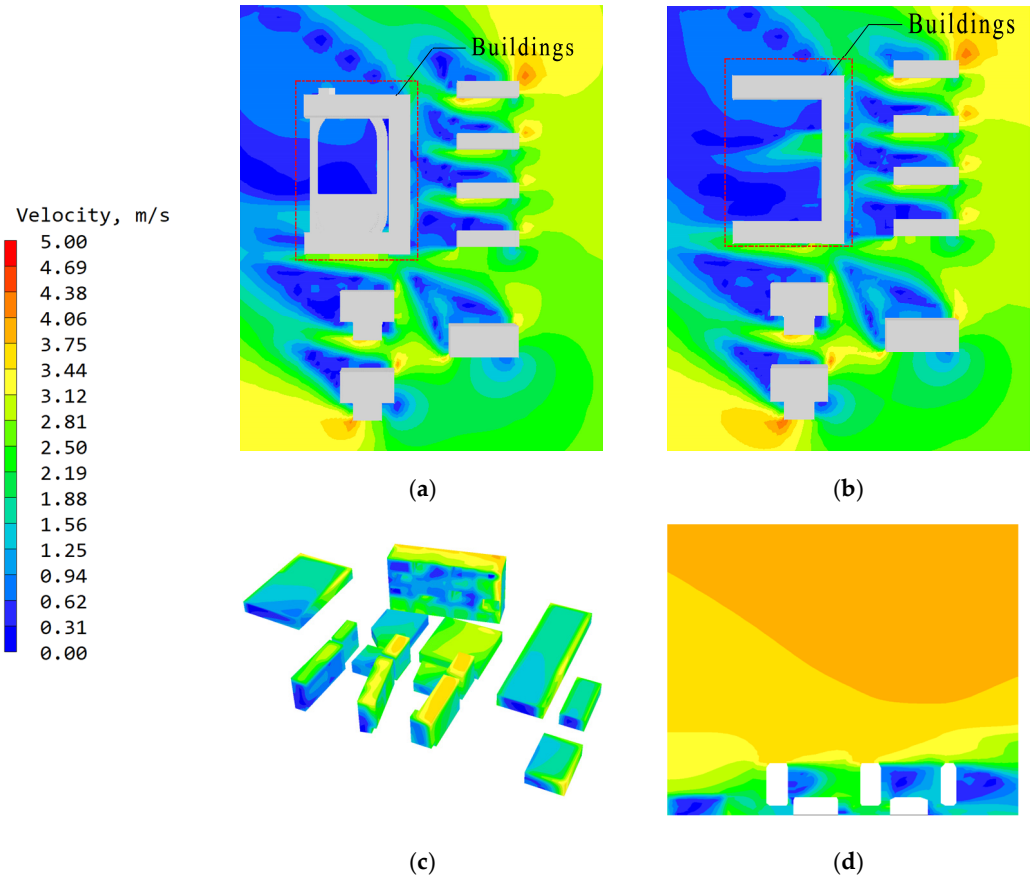

Note: The red dash line denotes the boundary of the school campus.

Figure 16. Multi-level and cross-sectional wind speed distributions of Pingshan Jinlong Primary School. (**a**) Wind speed distribution at the ground pedestrian level; (**b**) wind speed distribution at the elevated activity platform level; (**c**) wind speed contours on building surfaces; (**d**) longitudinal wind profile.

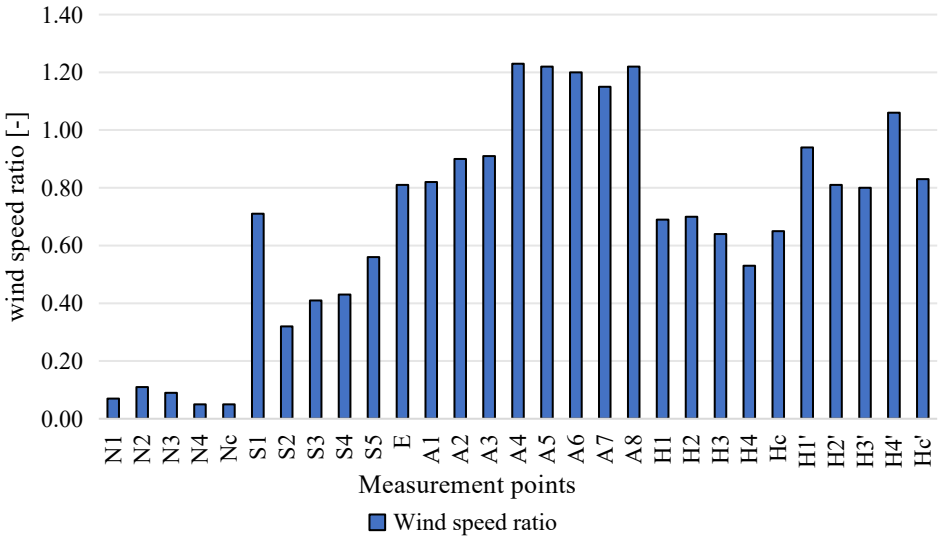

Figure 17. Comparison of wind speed ratios at different observation points of Pingshan Jinlong Primary School in summer.

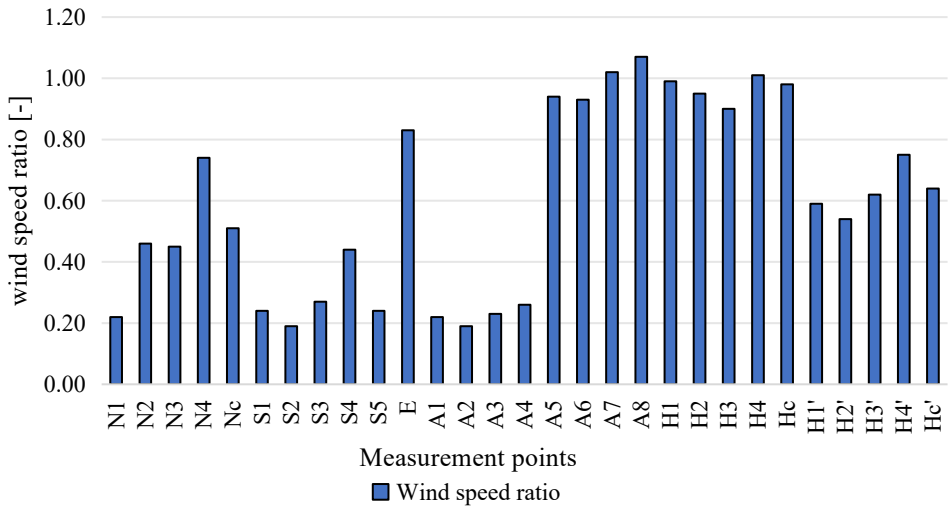

Figure 18. Comparison of wind speed ratios at different observation points of Pingshan Jinlong Primary School in winter.

5. Discussion

5.1. Research Subjects and Case Studies

The selection of primary school campuses as the research subject addresses the most acute shortage of school placements and construction challenges among the three types of compulsory education campuses, ensuring the theoretical relevance of this study. The findings offer theoretical guidance for designing typical high-density primary school campuses with the following characteristics: 36 classes, site areas of approximately 9400–16,000 m^2, building areas of 25,000–55,000 m^2, floor area ratios between 1.8 and 3.6, and 6 stories above ground. Furthermore, while most existing studies analyze individual design cases [50]—whose outcomes are often impacted by specific site conditions and surroundings, limiting the generalizability of their findings—this study draws from award-winning primary school campus designs in Shenzhen over the past four years. The adequate sample size and representative case selection enhance the scientific validity and transferability of the case study results.

5.2. Integration of High-Density Campus Layout and Wind Environment

This study specifically addresses the wind environment of high-density campuses in hot–humid climates. Through case studies and morphological analysis, we identify key morphological parameters that distinguish high-density from conventional campuses and propose fundamental spatial intensification strategies guided by wind comfort objectives. These are examined through three aspects: the degree of intensification in teaching building morphology, the openness of courtyard layouts, and the configuration of sports fields. This study employs four integrated indicators—average wind speed ratio, wind speed dispersion, wind comfort area ratio, and static wind area ratio—to comprehensively assess campus ventilation efficiency, wind environment stability, and outdoor comfort, thereby enriching the evaluation framework for wind environment performance.

The average wind speed ratios obtained in our simulations follow a descending order: parallel rows (0.69, Pingshan Jinlong) > continuous forms (0.54, Xinzhou) > centralized layouts (0.42, Renmin). These results align with the findings of Peng et al., who emphasized that in zigzag, branched, or enclosed layouts, reserving sufficiently large openings is essential to maintain smooth airflow and prevent localized stagnation [6]. Similarly, while compact or centralized arrangements tend to obstruct airflow and reduce pedestrian-level wind speeds, more dispersed layouts with aligned courtyards generally enhance ventilation. This is further supported by Deng et al., whose research indicated that staggered layouts and semi-enclosed courtyards significantly improve natural ventilation, particularly when apertures are aligned with the prevailing wind direction [8]. The relationship between layout and ventilation is nuanced; as noted by Du et al., different morphological patterns (such as fishbone versus matrix layouts) exhibit distinct localized effects. For instance, the canyon effect may not always yield the expected ventilation acceleration, as the efficiency of indoor and outdoor airflow is highly sensitive to specific opening designs and wind incidence angles [51].

Among the three morphological factors related to campus layout, the vertical position of the sports field impacts both the layout of teaching buildings and the spatial relationship between sports fields and teaching volumes, thereby affecting the overall wind environment. The intensification of the teaching building form, the openness of the courtyard layout, and the configuration of the sports field each differentially impact site ventilation, wind environment stability, and wind comfort. Specifically, the spatial relationship between the sports field and teaching buildings has a greater impact on ventilation efficiency and wind comfort area, while the vertical elevation of the sports field more significantly affects wind speed stability.

5.3. Limitations and Future Work

Firstly, the present work employs steady-state CFD simulations to identify comparative trends among different school layout typologies, with the scope deliberately focused on isolating the aerodynamic effects of fundamental architectural configurations. Consequently, several environmental factors present in real-world urban conditions—such as solar radiation, humidity, and the aerodynamic influence of vegetation—were not included in the current CFD model. These simplifications were necessary to establish a clear baseline understanding of wind-flow mechanisms at the pedestrian level.

Secondly, due to the absence of validation against on-site measured data, the conclusions of this study are primarily qualitative and comparative rather than absolute. While the steady-state simulation approach is widely adopted in pedestrian-level wind studies and is effective in identifying relative performance trends and causal relationships between layout and wind flow, it limits the direct quantification of physiological thermal comfort levels. To address this, future iterations of this methodology can be integrated with physi-

cal experiments, such as climate chamber simulations. Such an approach would provide a more robust portfolio of data to validate complex aerodynamic phenomena and thermal interactions in high-density urban contexts.

Therefore, the primary objective of this work was to identify key influencing factors and establish a foundational framework to guide subsequent, more detailed investigations. The findings successfully serve this purpose by pinpointing which layout parameters exert the most significant influence on pedestrian-level wind environments.

Future research will build directly upon these findings in three main directions: Future work will involve both wind tunnel testing and field measurement campaigns. Synchronized data on wind speed, air temperature, and turbulence intensity will be collected to provide a wider portfolio of information for calibrating the CFD models, ensuring the methodology's reliability across diverse urban landscapes and climate zones. Based on the validated models, more extensive parametric studies could be performed to develop quantified design guidelines or fast-assessment tools, providing data-driven recommendations for early-stage architectural design. In addition, future studies may integrate wind simulation results with physiological thermal comfort indices to provide a more holistic evaluation of outdoor microclimates, particularly under hot–humid climatic conditions. Overall, this study lays the necessary groundwork for these future efforts by identifying critical variables and relationships, ensuring that subsequent data collection and model refinement can be conducted in a targeted and efficient manner.

6. Conclusions

This study utilized steady-state CFD simulations to evaluate the impact of architectural layout on the outdoor wind environment in high-density primary school campuses in Shenzhen. Through a comparative analysis of typical cases, the research establishes qualitative correlations and identifies primary influencing factors, yielding the following conclusive findings:

(1) Quantifiable Performance Trends—The simulation results reveal clear quantitative trends: as the teaching building layout shifts from dispersed (e.g., parallel rows) to intensive (e.g., centralized), the average wind speed ratio decreases from approximately 0.69 to 0.42, while the static wind zone area ratio can increase dramatically from under 30% to over 58%. This confirms that building intensification significantly compromises site ventilation.

(2) Hierarchical Impact of Morphological Factors—The impact of the three morphological factors is distinct. The spatial relationship between the sports field and teaching buildings (juxtaposed vs. nested) has the most substantial impact on ventilation efficiency, leading to a variance of up to 22% in the wind comfort area ratio. In contrast, the vertical elevation of the sports field is the predominant factor affecting wind speed stability, with standard deviations of the wind speed ratio varying between 0.48 and 0.71.

(3) Actionable Design Strategies—Based on the above, the following design strategies are recommended to improve wind comfort: prioritize dispersed teaching building forms (e.g., parallel rows) over centralized types; orient courtyard openings towards the summer dominant wind direction (SE), and utilize semi-enclosed or three-sided enclosed forms; and juxtapose the sports field with teaching buildings rather than inserting it, and minimize its elevation above ground.

Author Contributions: Z.J.: Investigation, Data Curation, Resources, Writing—Original Draft Preparation; H.Z.: Validation, Formal Analysis, Data Curation, Visualization; L.S.: Methodology, Validation, Writing—Review and Editing, Formal Analysis.; J.W. (Jiantao Weng): Conceptualization, Methodol-

ogy, Supervision, Project Administration, Writing—Review and Editing; Q.C.: Methodology, Formal Analysis, Writing—Review and Editing; J.W. (Jindong Wu): Resources, Writing—Review and Editing; X.Y.: Conceptualization, Validation, Supervision, Project Administration, Writing—Review and Editing. All authors have read and agreed to the published version of the manuscript.

Funding: This research was funded by the Joint Fund of Zhejiang Provincial Natural Science Foundation of China under grant No. LLSSZ26F020002; 2023 Hangzhou major scientific and technological innovation projects in the fields of high-end equipment, new materials, and green energy (carbon peak and carbon neutrality): Research and integrated application of key technical equipment for urban and rural public buildings (No. 2023SZD0070); and the Hangzhou Joint Fund of the Zhejiang Provincial Natural Science Foundation of China under grant No. LHZY24A010004.

Data Availability Statement: The data presented in this study are available from the corresponding authors on request.

Conflicts of Interest: Author Zehua Ji and Hongbo Zhang were employed by the China Construction Science and Industry Corporation Limited. The remaining authors declare that the research was conducted in the absence of any commercial or financial relationships that could be construed as a potential conflict of interest.

Nomenclature

Symbol	Description	Unit
U_i, U_j	Mean velocity components	m/s
x_i, x_j	Coordinate directions	[-]
P	Pressure	Pa
ρ	Air density	kg/m^3
μ	Fluid dynamic viscosity	m^2/s
k	Turbulent kinetic energy	m^2/s^2
ε	Turbulent dissipation rate	m^2/s^3
C_μ, C_k, C_ε, $C_{\varepsilon 1}$, $C_{\varepsilon 2}$	Turbulence model constants	[-]
V_i	Wind speed at measurement point	m/s
V_0	Incoming wind speed	m/s
R_i	Wind speed ratio	[-]
σ	Standard deviation of wind speed ratio	[-]
μ	Mean wind speed ratio	[-]
S_C	Area with comfortable wind speed	m^2
S_F	Total site area	m^2
S	Wind comfort area ratio	%
S_{sw}	Static wind zone area	m^2
C	Static wind zone area ratio	%
H	Building height	m
δ_{ij}	Kronecker delta	[-]
$\overline{u_i u_j}$	Reynolds stress	m^2/s^2
S_{ij}	Mean strain rate tensor	s^{-1}
n	Number of measurement points	[-]
Re	Reynolds number	[-]
ν	Kinematic viscosity	m^2/s
α	Wind direction angle	°
T	Temperature	°C

References

1. Shenzhen Municipal Bureau of Statistics. Permanent Resident Population at Year-End. Available online: https://tjj.sz.gov.cn/ztzl/zt/sjfb/nmczrk/ (accessed on 24 January 2026).
2. Zhang, Z.; Luan, W.; Tian, C.; Su, M. Impact of Urban Expansion on School Quality in Compulsory Education: A Spatio-Temporal Study of Dalian, China. *Land* **2025**, *14*, 265. [CrossRef]
3. Zhou, H. Futian New Campus Action Plan: From Hongling Experimental Primary School to "8 + 1" Joint Architecture Exhibition. *Archit. J.* **2021**, 54–61. (In Chinese) [CrossRef]
4. Meteorological Bureau of Shenzhen Municipality. *Shenzhen Climate Bulletin 2022*; Meteorological Bureau of Shenzhen Municipality: Shenzhen, China, 2023. Available online: https://weather.sz.gov.cn/attachment/1/1241/1241864/10407891.pdf (accessed on 24 January 2026).
5. Juan, Y.H.; Aspriyanti, V.A.; Chen, W.Y. Wind Flow Characteristics in High-Rise Urban Street Canyons with Skywalks. *Phys. Fluids* **2025**, *37*, 035160. [CrossRef]
6. Peng, Z.; Jiang, M.; Liu, M.; He, T.; Jiang, N.; Huan, X. An Investigation into the Effects of Primary School Building Forms on Campus Wind Environment and Classroom Ventilation Performance. *Appl. Sci.* **2024**, *14*, 7174. [CrossRef]
7. Wu, Z.; Zhang, Y.; Mai, J.; Wang, F.; Zhai, Y.; Zhang, Z. Adaptation-based Indoor Environment Control with Night Natural Ventilation in Autumn in an Office Building in a Hot-Humid Area. *Build. Environ.* **2023**, *243*, 110702. [CrossRef]
8. Deng, J.; Xia, Y.; Lao, H.; Ye, Y.; Wang, Z.; Jiang, H. Natural Ventilation Potential of Teaching Building Complexes with Different Block Shapes and Layout Patterns. *J. Build. Eng.* **2024**, *96*, 110420. [CrossRef]
9. Xu, F.; Liu, Q. Building Energy Consumption Optimization Method based on Convolutional Neural Network and BIM. *Alex. Eng. J.* **2023**, *77*, 407–417. [CrossRef]
10. Su, X.; Tao, Z. Research on the Design Strategies of Comprehensive Primary and Secondary School Campus in Urban City. *South Archit.* **2020**, *01*, 73–80. (In Chinese)
11. Aguilar, A.; de la Hoz-Torres, M.; Costa, N.; Arezes, P.; Martínez-Aires, M.D.; Ruiz, D. Assessment of ventilation rates inside educational buildings in Southwestern Europe: Analysis of implemented strategic measures. *J. Build. Eng.* **2022**, *51*, 104204. [CrossRef]
12. Zhang, Y.; Guo, Z.; Zhuo, L.; An, N.; Han, Y. Ventilation Strategies for Highly Occupied Public Environments: A Review. *Buildings* **2023**, *13*, 1642. [CrossRef]
13. Elshabshiri, A.; Aly, M.; Alharbat, R.; Abdalla, M.; Alsyouf, L.; Ghanim, A.; Yahia, M. Enhancing the Microclimate of Outdoor Campus Spaces in Hot Humid Climates: The Example of the University of Sharjah. *Comput. Urban Sci.* **2025**, *5*, 35. [CrossRef]
14. Son, S.; Jang, C.M. Air Ventilation Performance of School Classrooms with Respect to the Installation Positions of Return Duct. *Sustainability* **2021**, *13*, 6188. [CrossRef]
15. Liu, X.; Yang, L.; Qian, F. Study on Ventilation Conditions for Different Types of Teaching Buildings. *Build. Sci.* **2019**, *35*, 102–109. (In Chinese) [CrossRef]
16. Hou, H.; Yang, D. Study on the Campus Planning of Primary and Middle Schools under a High-Density Environment. *South Archit.* **2018**, 81–86. (In Chinese)
17. Liu, X.; Yang, L. Research on Environmental Adaptability of Ecological Space in Green Campus. *Build. Sci.* **2021**, *37*, 111–119. (In Chinese) [CrossRef]
18. Chen, S.; Chen, C. Primary and Middle School Building Layout Based on Wind Environment Simulation: Case analysis in Guangzhou. *Build. Energy Effic.* **2021**, *49*, 33–41. (In Chinese)
19. *GB 50099-2011*; Code for Design of Schools. Ministry of Housing and Urban-Rural Development of the People's Republic of China: Beijing, China; China Architecture & Building Press: Beijing, China, 2011. (In Chinese)
20. Xiao, Y.; Zou, Y.; Xiao, Y. Overlaid Campus: Building a Campus for Break Time Between Classes in an Urban Environment of High Density The Design of Xinzhou Primary School, Futian district, Shenzhen. *Archit. J.* **2021**, 27–34. (In Chinese) [CrossRef]
21. Du, Y.; Mak, C.; Liu, J.; Xia, Q.; Niu, J.; Kwok, K. Effects of Lift-Up Design on Pedestrian Level Wind Comfort in Different Building Configurations under Three Wind Directions. *Build. Environ.* **2017**, *117*, 84–99. [CrossRef]
22. Andamon, M.; Rajagopalan, P.; Woo, J. Evaluation of Ventilation in Australian School Classrooms Using Long-term Indoor CO2 Concentration Measurements. *Build. Environ.* **2023**, *237*, 110313. [CrossRef]
23. Shenzhen Municipality Bureau of Statistics; Survey Office of the National Bureau of Statistics in Shenzhen. *Shenzhen Statistical Yearbook 2022*; China Statistics Press: Shenzhen, China, 2023. Available online: https://www.sz.gov.cn/attachment/1/1582/1582340/10390921.pdf (accessed on 24 January 2026). (In Chinese)
24. CHAM. *PHOENICS 2019 Software*; Concentration, Heat and Momentum Limited (CHAM): London, UK, 2019. Available online: https://www.cham.co.uk (accessed on 24 January 2026).

25. Fang, H.; Yang, Y.; Wang, J.; Ji, X. Study on the Adaptation of the Outdoor Wind Environment of Xuzhou Rural Residence. *Sci. Rep.* **2025**, *15*, 23798. [CrossRef]
26. *DBJ/T 15-154-2019*; Testing and Assessment Standard for Building Wind Environment. Guangdong Provincial Department of Housing and Urban-Rural Development: Guangzhou, China; China City Press: Beijing, China, 2019. (In Chinese)
27. Li, Q.; Mochida, A.; Meng, Q.; Zhao, L. Comparison of Turbulence Models for Numerical Simulation of Outdoor Wind Environment around Building. *J. South China Univ. Technol. (Nat. Sci. Ed.)* **2011**, *39*, 121–127. (In Chinese) [CrossRef]
28. Wang, Z.; Wang, M.; Huang, T.; Wang, Y.; Zeng, Y.; Vishnupriya, V.; Shen, X. Evaluation of the Influence of Traditional Village Square Layout Factors on Wind Comfort. *Build. Environ.* **2025**, *267*, 112160. [CrossRef]
29. Architectural Institute of Japan. *Guidebook for CFD Predictions of Urban Wind Environment*; Architectural Institute of Japan: Tokyo, Japan, 2020. Available online: https://www.aij.or.jp/jpn/publish/cfdguide/index_e.htm (accessed on 19 January 2026).
30. Ju, P.; Li, M.; Wang, J. Review of Research Advances in CFD Techniques for the Simulation of Urban Wind Environments. *Fluid Dyn. Mater. Process.* **2022**, *18*, 449–462. [CrossRef]
31. Baetke, F.; Werner, H.; Wengle, H. Numerical Simulation of Turbulent Flow over Surface-Mounted Obstacles with Sharp Edges and Corners. *J. Wind Eng. Ind. Aerodyn.* **1990**, *35*, 129–147. [CrossRef]
32. Li, Z.; Zhang, H.; Wen, C.Y.; Yang, A.S.; Juan, Y.H. Effects of frontal area density on outdoor thermal comfort and air quality. *Build. Environ.* **2020**, *180*, 107028. [CrossRef]
33. Reiminger, N.; Wemmert, C.; Maurer, L.; Vazquez, J.; Jurado, X. Breaking the Isothermal Assumption in CFD Air Quality Modeling: Solar Irradiance Effects on the Wind Velocity-Concentration Relationship. *Sustain. Cities Soc.* **2026**, *137*, 107135. [CrossRef]
34. Franke, J.; Hirsch, C.; Jensen, G.; Krüs, H.W.; Miles, S.D.; Schatzmann, M.; Westbury, P.S.; Wisse, J.A.; Wright, N. Recommendations on the Use of CFD in Wind Engineering: Conference; COST Action C14, Impact of Wind and Storm on City Life and Built Environment. In Proceedings of the International Conference on Urban Wind Engineering and Building Aerodynamics, Sint-Genesius-Rode, Belgium, 5–7 May 2004; pp. C.1.1–C1.11.
35. *JGJ/T 449-2018*; Standard for Green Performance Calculation of Civil Buildings. Ministry of Housing and Urban-Rural Development of the People's Republic of China: Beijing, China; China Architecture & Building Press: Beijing, China, 2018. (In Chinese)
36. Launder, B.; Spalding, D.B. *Lectures in Mathematical Model of Turbulence*; Academic Press: Cambridge, MA, USA, 1972.
37. Spalding, D.; Launderd, B. The Numerical Computation of Turbulent Flows. In *Numerical Prediction of Flow, Heat Transfer, Turbulence and Combustion*; Elsevier: Amsterdam, The Netherlands, 1983; pp. 96–116. [CrossRef]
38. Shih, T.; Liou, W.; Shabbir, A.; Yang, Z.; Zhu, J. A New K-ϵ Eddy Viscosity Model for High Reynolds Number Turbulent Flows. *Comput. Fluids* **1995**, *24*, 227–238. [CrossRef]
39. Chen, G.; Hang, J.; Chen, L.; Lin, Y. Comparison of Uniform and Non-Uniform Surface Heating Effects on in-Canyon Airflow and Ventilation by CFD Simulations and Scaled Outdoor Experiments. *Build. Environ.* **2023**, *244*, 110744. [CrossRef]
40. Antoniou, N.; Montazeri, H.; Wigo, H.; Neophytou, M.K.-A.; Blocken, B.; Sandberg, M. CFD and Wind-Tunnel Analysis of Outdoor Ventilation in a Real Compact Heterogeneous Urban Area: Evaluation Using "Air Delay". *Build. Environ.* **2017**, *126*, 355–372. [CrossRef]
41. Liang, G.; Cui, D.; Mak, C.M.; Kwok, K. Evaluating the Effects of Envelope Features on the Pollutant Distribution and Ventilation Performance by CFD Simulations and Scaled Outdoor Experiments. *Build. Environ.* **2024**, *264*, 111947. [CrossRef]
42. He, K.; Gan, L.; Zhou, H. Standardization Process of Wind Environmental Simulation in Green Building. *Build. Energy Effic.* **2011**, *39*, 22–24. (In Chinese) [CrossRef]
43. Shi, X.; Li, Y. Evaluation Criteria and Methodology for Pedestrian-Level Wind Environment in Urban Design. *J. Hum. Settl. West China* **2015**, *30*, 22–27. (In Chinese) [CrossRef]
44. Janssen, W.D.; Blocken, B.; Van Hooff, T. Pedestrian Wind Comfort around Buildings: Comparison of Wind Comfort Criteria based on Whole-Flow Field Data for a Complex Case Study. *Build. Environ.* **2013**, *59*, 547–562. [CrossRef]
45. Cheng, V.; Ng, E. Thermal Comfort in Urban Open Spaces for Hong Kong. *Archit. Sci. Rev.* **2006**, *49*, 236–242. [CrossRef]
46. *GB/T 19201-2006*; Grage of Tropical Cyclones. Standards Press of China: Beijing, China, 2006. (In Chinese)
47. Pang, Y.; Liang, Z.; Xie, P.; Li, L. Adaptive Optimization of Wind Environment in Coastal Village Spatial Forms of Western Guangdong. *Buildings* **2024**, *14*, 3721. [CrossRef]
48. Liu, S.; Pan, W.; Zhang, H.; Cheng, X.; Long, Z.; Chen, Q. CFD Simulations of Wind Distribution in an Urban Community with a Full-Scale Geometrical Model. *Build. Environ.* **2017**, *117*, 11–23. [CrossRef]
49. Blocken, B. Computational Fluid Dynamics for Urban Physics: Importance, Scales, Possibilities, Limitations and Ten Tips and Tricks towards Accurate and Reliable Simulations. *Build. Environ.* **2015**, *91*, 219–245. [CrossRef]

50. Talwar, T.; Yuan, C. Impact of Natural Urban Terrain on the Pedestrian Wind Environment in Neighborhoods: A CFD Study with both Wind and Buoyancy-driven Scenarios. *Build. Environ.* **2024**, *261*, 111746. [CrossRef]
51. Du, Z.; Guo, W.; Li, W.; Gao, X. A Study on the Optimization of Wind Environment of Existing Villa Buildings in Lingnan Area: A Case Study of Jiangmen's "Yunshan Poetic" Moon Island Houses. *Buildings* **2022**, *12*, 1304. [CrossRef]